Notes for three lectures on topological fluid waves - Draft version

A. Venaille

July 20, 2022

Contents

Introduction (slides)

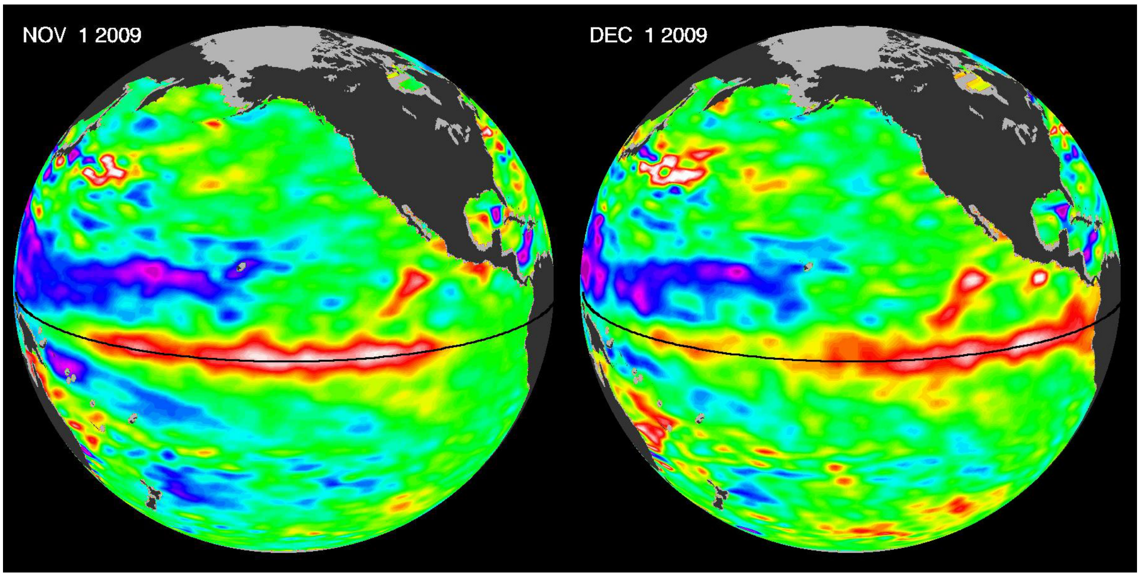

Figure 1: **Equatorial Kelvin wave.** Propagation of a temperature anomaly in Pacific ocean between November 1st (left) and December 1st (right). Red color corresponds to around $+2$ degree Celsius anomalies. The arrival of hot temperature anomalies along the coast of Peru corresponds to the beginning of El Nino phenomenon. Remarkably, this wave can only propagate energy eastward. This is in stark contrast wit our intuition of small scale water waves that are emitted in all directions when we throw a stone in the sea. There is only two wave modes that share this remarkable property of being unidirectional. Why? Topology! See lecture 1 for the theory, and the appendix for more details on observations. *Image: Courtesy NASA/JPL-Caltech. Source: Jet Propulsion Laboratory.*

Phenomena: unidirectional edge modes (figure 1

- El Nino: two unidirectional trapped modes along the equator. Why?
- Tides: one unidirectional trapped mode along coast. Why?
- Chiral modes in films of He3-A. Is it different?
- A detour through topological insulators.

Topology

- Classifies objects into families
- Bundle of vectors
- Why are those tools useful for hydrodynamics across scales?

Outline

Reading list complementary to these lecture notes

- Delplace lecture notes SciPost 2021
- Faure lecture notes ArXiv 2019
- Perez PhD thesis 2022 to be available soon online.
- A nice introductory movie "The Hairy Nobel" (French with english subtitles):

  `https://www.youtube.com/watch?v=gEnDNUfGQTQ`

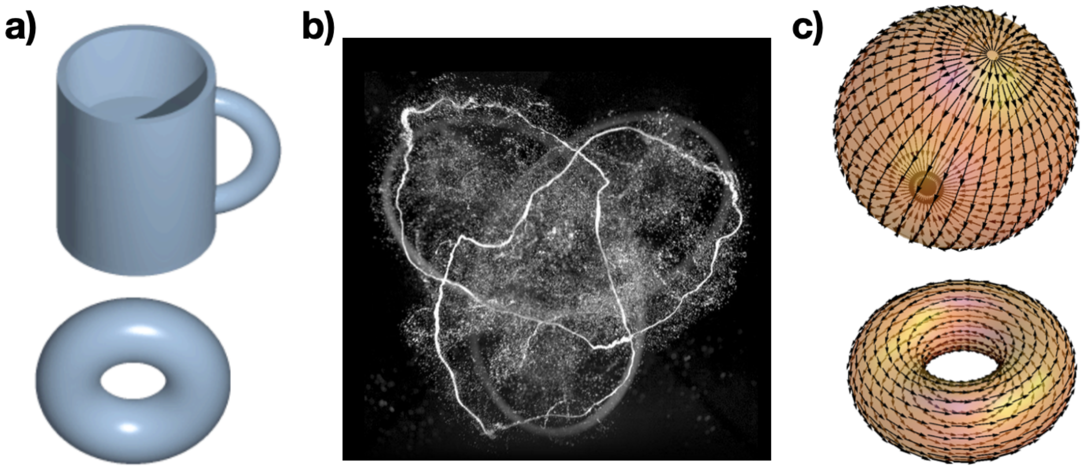

Figure 2: Topology classifies objects into family that share common properties. In a given familly, the members can be deformed continuously from one to another. This allows to transform complicated problems into simpler ones. A fex examples are **a)** closed 2D surfaces, *from wikipedia*) **b)** knots and links, as here observed in a vorticity filament. *Figure taken from Kleckner et al Nature 2013, W. Irvine group.* **c)** Bundle of vectors over a closed surface, as for instance a field of tangent vectors to the surface. Note the presence of singularities in the sphere, not on the torus. This number is a topological invariant: one can make different choices of tangent vectors, the singularity will move somewhere else but will not disappear. *Figure taken from David Carpentier lectures.* **This lecture will be devoted to such vector bundles,** albeit in an abstract 3D parameter space, with vectors being complex. Indeed, we will describe fluid wave eigenmodes, and describe how twisted are familly of eigenmodes when parameters are varied. **What is the relation between such abstract objects and unidirectional modes?** The answer will be given by a bulk-interface correspondence that will be explained in these lectures.

1 Lecture 1: topological origin of equatorial waves

1.1 Objectives

- Introduce rotating shallow water flow models.
- Introduce the concepts of spectral flows, Chern number, Berry monopole and bulk-boundary correspondence.
- Describe the equatorial shallow wave problem as a manifestation of an index theorem.

This first lecture is based on a paper with P. Delplace and B. Marston, Science 2017

1.2 From tides to ElNino: discovery of the equatorial waveguide

- **Laplace 1799** on dynamical tides *Sur les flux et reflux de la mer* introduces a shallow water wave model on a spherical rotating planet with rotation vector $\mathbf{\Omega}$, as displayed figure 3. His model features a Coriolis force terms before its introduction by Coriolis! A central parameter of the problem is the **Coriolis parameter**

$$f = 2\mathbf{\Omega} \cdot \mathbf{e}_z \tag{1}$$

with $\mathbf{\Omega}$ the planet rotation vector and $\mathbf{e}_z$ a normal vector pointing in vertical direction (given by gravity).

- **Kelvin 1880** simplifies the problem: he assumes that the dynamics takes place in a plane tangent to the Earth, with

$$f = cst \tag{2}$$

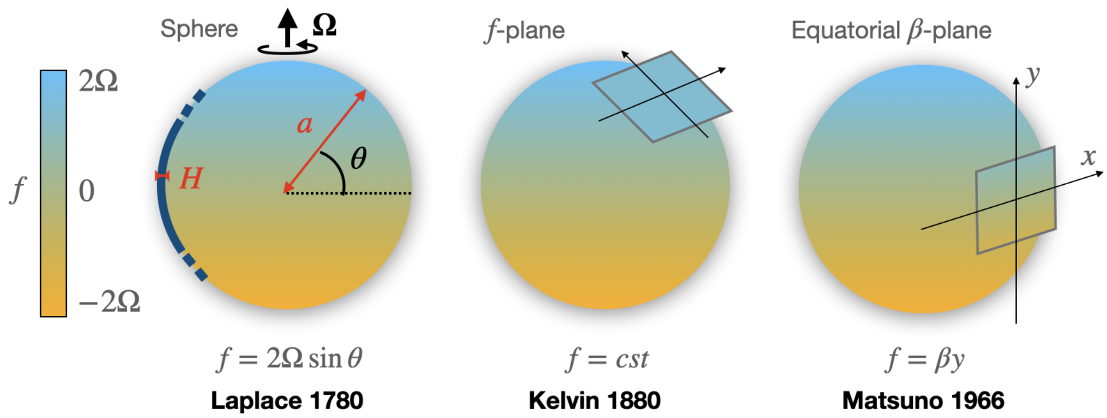

Figure 3: Coriolis parameter f, from Laplace tidal equations to the equatorial beta plane. In Laplace and Matsuno case, the equator $f(0) = 0$ defines an interface between a Northern hemisphere ($f > 0$) and a Southern hemisphere $f < 0$. *The existence of such an interface will play a central role in this lecture.*

This simplification is extremely useful, and is now called the ***f*-plane approximation**. It leads to a solvable model and an insightful description of rotating shallow water waves to be described in this lecture.

- **Matsuno 1966** makes a step change in our understanding of planetary waves by assuming as Kelvin that the dynamics takes plane in a plane tangent to the earth, while taking into account variations of Coriolis parameter with latitude. By assuming

$$f = \beta y \tag{3}$$

  with y the coordinate in meridional direction, he obtained another solvable case, to be described in this lecture. This configuration is now called **the equatorial beta plane.** He found that the equator acts are a waveguide, and predicted the existence of two unidirectional trapped modes.

- Matsuno computation has been a triumph of geophysical fluid dynamics, as those waves have been observed a few years after. Matsuno paper has been very influential in the next decades, as the waves he found are the building block of most climate phenomena taking place in the equatorial area. In particular one of the uni-directional modes discovered by Matsuno is now routinely observed as a warm temperature anomaly in the upper layer of Pacific ocean propagating eastward from Indonesia to Peru in about one month before an El Nino event. See figure 19 in the appendix of this lecture to see how well linear theory can be for real planetary scale atmospheric equatorial waves.

This short historical timeline gives the outline of today's lecture, with a twist: we will see that Matsuno spectrum could have been deduced from Kelvin computations, if topological waves were known at that time. In fact, those tools started to emerge in mathematics in the sixties (Atiyah Singer index theorems), and in condensed matter in the eighties (interpretation of quantized Hall effect with topological invariants).

1.3 Shallow water equations on a tangent plane

Flow model. Consider a thin layer of fluid with homogeneous density, on a flat bottom, with a free surface, as displayed figure 4. The layer thickness is denoted

$$h(x, y, t) = \eta(x, y, t) + H, \tag{4}$$

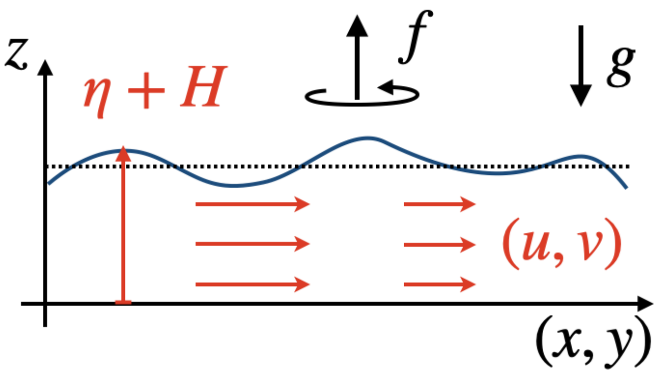

Figure 4: Shallow water model: a thin layer of incompressible fluid of constant density with depth H much smaller than horizontal scales of motion. Note that only the horizontal component of Coriolis force is taken into account. This is called the traditional approximation.

where H is the mean thickness of the fluid layer, much smaller than horizontal scales of motion denoted L. Starting from 3D Euler equations, imposing a no-normal flow condition at the bottom, a condition of constant pressure above the fluid layer, and taking the shallow water limit $H/L \ll 1$ leads to

- hydrostatic balance on the vertical
- a depth-independent horizontal velocity field denoted (u, v).
- a dynamical system given by mass and horizontal momentum conservation:

$$\partial_t u + u\partial_x u + v\partial_y u = -g\partial_x h + fv, \tag{5}$$
$$\partial_t v + u\partial_x v + v\partial_y v = -g\partial_y h - fu, \tag{6}$$
$$\partial_t h + \partial_x(uh) + \partial_y(vh) = 0, \tag{7}$$

where g is the gravity and f is the Coriolis parameter.

Linearization around a state at rest. From now on, we neglect nonlinear terms, together with the following rescaling:

$$u' = \frac{u}{c}, \quad v' = \frac{v}{c}, \quad \eta' = \frac{h - H}{H}, \quad c \equiv \sqrt{gH}. \tag{8}$$

We get the central wave problem to be studied these lectures:

$$\frac{\partial}{\partial t}\begin{pmatrix} u' \\ v' \\ \eta' \end{pmatrix} = \begin{pmatrix} 0 & f(y) & -c\frac{\partial}{\partial x} \\ -f(y) & 0 & -c\frac{\partial}{\partial y} \\ -c\frac{\partial}{\partial x} & -c\frac{\partial}{\partial y} & 0 \end{pmatrix}\begin{pmatrix} u' \\ v' \\ \eta' \end{pmatrix}, \tag{9}$$

It is the simplest version of Laplace tidal equation, without forcing and dissipation terms. Solving this wave problem amounts to find free modes (pulsations) of the ocean.

1.4 The bulk: shallow water waves on the f-plane (aka Kelvin problem)

Here we consider the case of an unbounded plane with f constant. Owing to the homogeneity of the wave equations, eigenmodes are simply Fourier modes

$$(u', v', \eta') = (\hat{u}, \hat{v}, \hat{\eta})e^{ikx+ily-i\omega t} + c.c. \tag{10}$$

Injecting this expression into (9) turn the computation of f-plane waves into a matrix problem:

$$\omega\begin{pmatrix} \hat{u} \\ \hat{v} \\ \hat{\eta} \end{pmatrix} = \begin{pmatrix} 0 & if & ck \\ -if & 0 & cl \\ ck & cl & 0 \end{pmatrix}\begin{pmatrix} \hat{u} \\ \hat{v} \\ \hat{\eta} \end{pmatrix}, \tag{11}$$

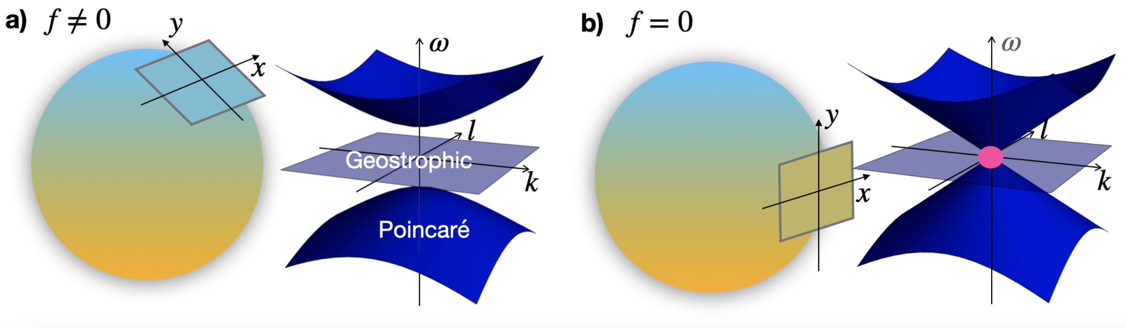

Figure 5: Dispersion relation of rotating shallow water waves on an unbounded f-plane (Kelvin problem). The three-fold degeneracy point is emphasized with a pink thick point. *This degeneracy point will play a central role in this lecture.*

Dispersion relation Given that three fields are involved, one finds three eigenvalues denoted $(\omega_-, \omega_0, \omega_+)$, that correspond to three wavebands when parameters (k, l) are varied, with dispersion relation

$$\omega_0 = 0, \quad \omega_\pm = \pm\sqrt{f^2 + c^2k^2 + c^2l^2}. \tag{12}$$

This dispersion relation is displayed figure 5. Note that the system is a kind of insulator: no wave can propagate within the frequency gap $|\omega| \in]0, f[$.

Geostrophic modes. The flat band $\omega_0 = 0$ correspond to stationary waves called geostrophic modes, as the corresponding eigenmodes are geostrophically balanced with $f(u', v') = c(-\partial_y\eta',\ \partial_x\eta')$. Think of midlatitude weather maps, where pressure lines are interpreted as streamlines.

Inertia-gravity wave modes. Geostrophic modes are separated from positive and negative frequency inertia-gravity wave bands $\omega_\pm$ by the frequency gap of size f. The inertia-gravity wave modes correspond to the familiar surface waves whose dispersion relation is modified by rotation. They are also called Poincaré, Sverdrup or simply gravity wave modes. Remember that any real mode solution is a combination of a mode (ω, k) with its complex conjugate $(-\omega, -k)$, so that a given real inertia gravity-wave mode involve both the positive and negative frequency inertia-gravity wave bands.

A singularity at the equator. The equatorial f-plane is peculiar, as the frequency gap between wavebands closes when $f = 0$: a three-fold degeneracy point occurs at the origin $(k, l) = (0, 0)$, as displayed figure 5b. We will see that this band-touching point is an obstruction to smoothly deform the family of f-plane eigenmodes from one hemisphere to another. This singularity will plays a key role in these lectures.

Q): *Interpret the symmetries observed in the dispersion relation. See next lecture for the answer.*

1.5 The interface: equatorial β-plane (aka Matsuno problem)

Equatorial beta-plane. To take into account the effect of the planet rotation on a plane tangent to the equator, one needs to consider the variations of the Coriolis parameter with latitude. Matsuno considered the simplest possible configuration allowing for explicite computations, namely linear variations of the Coriolis parameter with latitude: $f = \beta y$.

A 1D wave multicomponent wave equation. The main difficulty with respect to the f-plane case is that the linear operator in Eq. (9) now depends on y. Owing to the translational invariance in the x-direction only, eigenmodes are expressed as

$$(u, v, \eta) = (\hat{u}(y), \hat{v}(y), \hat{\eta}(y))\, e^{ikx - i\omega t} + c.c.\ . \tag{13}$$

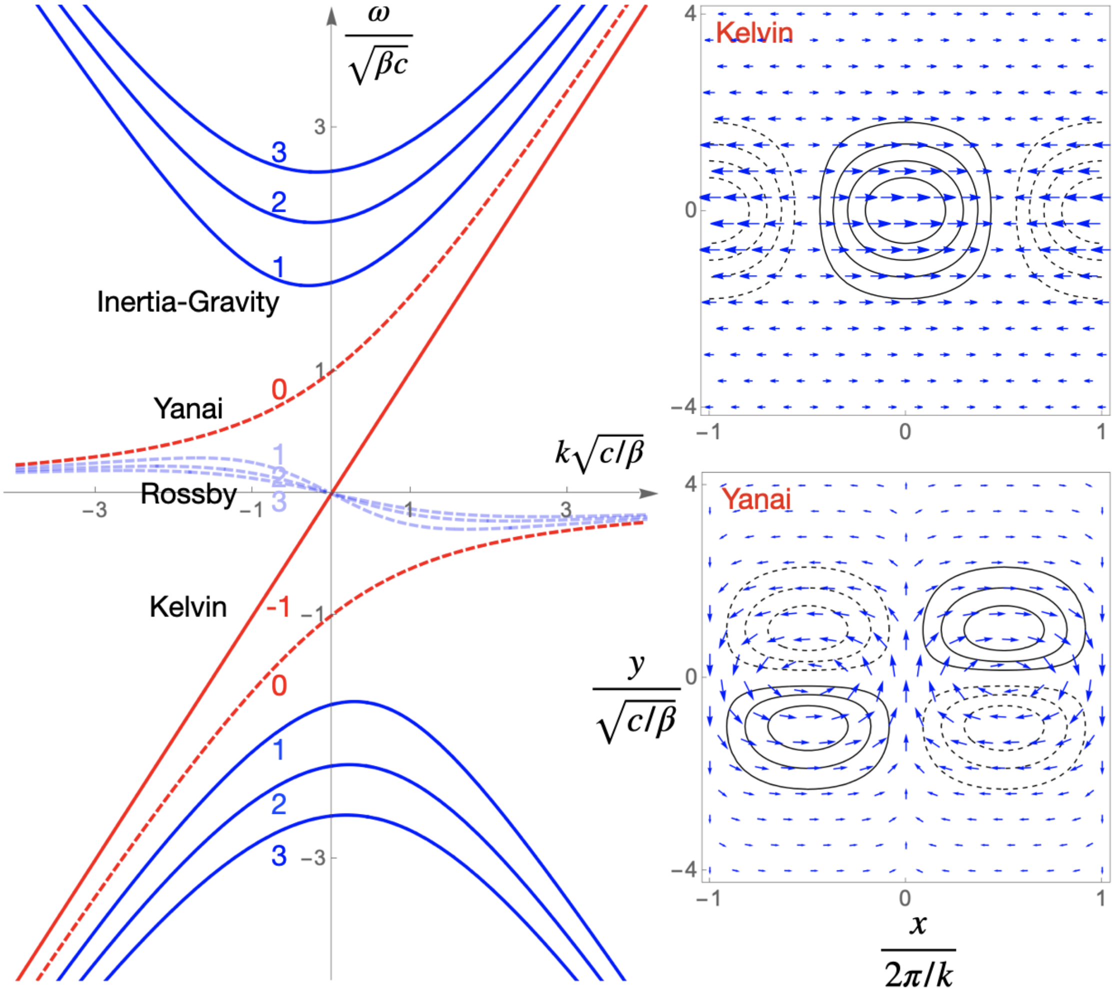

Figure 6: Dispersion relation of equatorial shallow water waves on the beta plane (Matsuno spectrum).

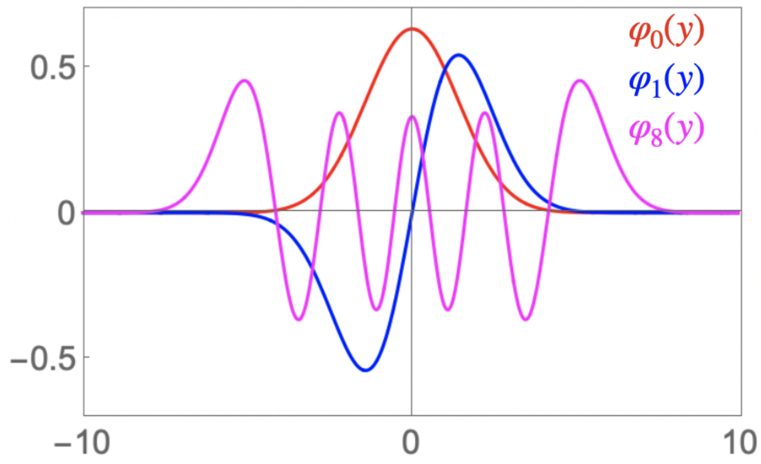

Figure 7: Normalized profiles of **parabolic cylinder functions** $\varphi_n(y)$ defined in (16).

The linearized dynamic (9) is then recast as an eigenvalue problem for the frequency ω:

$$\omega \begin{pmatrix} \hat{u} \\ \hat{v} \\ \hat{\eta} \end{pmatrix} = \begin{pmatrix} 0 & i\beta y & ck \\ -i\beta y & 0 & -ic\frac{\partial}{\partial y} \\ ck & -ic\frac{\partial}{\partial y} & 0 \end{pmatrix} \begin{pmatrix} \hat{u} \\ \hat{v} \\ \hat{\eta} \end{pmatrix} . \tag{14}$$

The problem admits a intrinsic time and length scale given by $1/\sqrt{\beta c}$, and $\sqrt{c/\beta}$, respectively. From now on, we choose them to be one. The problem was solved by Matsuno, and the result is plotted figure 6. It is useful to give some details on the computation that leads to this spectrum.

Mapping to the quantum harmonic oscillator. After some manipulations, one finds that the meridional velocity satisfies

$$\frac{\mathrm{d}^2 \hat{v}}{\mathrm{d}y^2} + \left(\omega^2 - k^2 - \frac{k}{\omega} - y^2 \right) \hat{v} = 0 \ , \tag{15}$$

with the condition that v vanishes at large $|y|$. This equation is formally analogous to the celebrated 1D quantum harmonic oscillator, whose solutions are well documented.

Trapping of the waves. To compute these solutions, it is convenient to project the field v onto a basis of parabolic cylinder functions displayed figure 7, and defined as

$$\varphi_n(y) = H_n\,(y)\, e^{-\frac{1}{2}y^2}, \quad n \in \mathbb{N}. \tag{16}$$

The functions $H_n(y)$ are Hermite polynomials of order n: $H_0 = 1$, $H_1 = 2y$, etc.. In dimensional units, the trapping length scale is $\sqrt{c/\beta}$. It is called the equatorial Rossby radius of deformation.

Quantized dispersion relation Each basis element φ_n is a solution of Eq. (15) provided that

$$\omega^2 - k^2 - \frac{k}{\omega} = 2n + 1, \tag{17}$$

which is the equatorial counterpart of energy quantization in the quantum harmonic oscillator case. By constrast with the f-plane, the spectrum is discrete.

Important warning: this is a multicomponent wave problem Equation (15) also involves the fields u and η, which can be deduced from v by solving

$$(\omega - k)\,(\hat{u} + \hat{\eta}) = i\,(y - \partial_y)\,\hat{v} \tag{18}$$

$$(\omega + k)\,(\hat{u} - \hat{\eta}) = i\,(y + \partial_y)\,\hat{v}. \tag{19}$$

***Q**) check that $\omega = \pm k$ are not admissible solutions if $v = \varphi_n$, as it would imply the divergence of u and η.*

We have now introduced all the tools required to describe the whole spectrum, which is displayed figure 6.

Inertia-gravity and Rossby waves. When $n \geq 1$, the three solutions of Eq (17) all satisfy $\omega \neq \pm k$, and one get for each value of zonal wavenumber k a triplet ofsolutions, just as in the f-plane configuration. The two high frequency modes with opposite signs correspond to inertia-gravity waves. The remaining low frequency solution is close to geostrophic balance, and can thus be identified to the f-plane geostrophic wave band. Neglecting the term ω^2 in Eq (17), one recovers the dispersion relation of Rossby waves encountered in Tiffany Shaw lectures

Yanai waves. The case $n = 0$ in Eq. (17) is special: one of the three possible roots is $\omega = -k$, which, according to Eq. (18-19), is not an admissible solution. There is thus only two solutions, that can be recombined into one negative frequency and one positive frequency branch in the dispersion relation.

Kelvin waves. The last class of modes is obtained by looking for solutions satisfying $\hat{v} = 0$. Check that the only possible solution is $\hat{u} = \hat{\eta} = \varphi_0$ with $\omega = ck$. The name of this wave mode comes from its strong similarities with unidirectional trapped modes along a coast originally computed by Kelvin (see lecture 2). This mode is sometimes labelled by the index $n = -1$, as $\omega = k$ is one of the root of Eq. (17).

Polarization relation You may recognize in the r.h.s. of (18)-(19) the anihilation and creation operator of quantum mechanics. If not, just recall the following property of parabolic cylinder functions:

$$(y - \partial_y)\,\varphi_n = \varphi_{n+1}, \quad (y + \partial_y)\,\varphi_n = 2n\varphi_{n-1}, \quad (y + \partial_y)\,\varphi_0 = 0. \tag{20}$$

The polarization relation for all the modes is conveniently expressed as

$$\begin{pmatrix} u+\eta \\ v \\ u-\eta \end{pmatrix} = \begin{pmatrix} i(\omega+k) & 0 & 0 \\ 0 & \omega^2 - k^2 & 0 \\ 0 & 0 & 2ni(\omega-k) \end{pmatrix} \begin{pmatrix} \varphi_{n+1} \\ \varphi_n \\ \varphi_{n-1} \end{pmatrix}, \tag{21}$$

assuming the notation $\varphi_{-1} = \varphi_{-2} = 0$. Owing to the Hermiticity of the operator, the whole set of eigenmodes is a basis for all triplet of fields. Look at how this basis is organized, by comparison with three independent basis of parabolic cylndrical functions $\{\varphi_n\}_{n\in\mathbb{N}}$ for each fields of the triplet (FIGURE).

Spectral flow. The Yanai and Kelvin branches in the dispersion relation transit from one wave band to another when k is varied. This is called a spectral flow. A **spectral flow index** can be ascribed to each waveband. It counts the net number of modes gained (or lost) as k is increased. For instance, **the spectral flow index for positive inertia-gravity wave band in Matsuno problem is 2. Our aim here is to understand the origin of this number.**

We explain in the next section that such spectral flow index could actually have been deduced directly from the study of the simpler Kelvin' bulk problem, using a deep mathematical result that relates this spectral index to a topological index.

1.6 Back to the bulk: useful information is encoded in eigenmodes.

When discussing Kelvin wave problem, we focused on the dispersion relation. We forgot on the way an important part of the matrix problem: the eigenvectors! The main message of todays's lecture is

To understand the global shape of dispersion relation in (complicated) interface problems, just look at the topology of bulk eigenvectors, that are much simpler to compute.

Our aim, now, is to focus on such eigenvectors, which give the wave polarization relation of bulk waves (the relation between u, v and η). When parameters such as f, k or l are varied, the polarization relation changes. When parameters are varied over a 3D space, the set of eigenvectors spanned by those parameters may be twisted. This precisely what we would like to describe. Before this, let us recall informally some important notions encountered in topology.

Topology of surfaces. Topology classifies objects into families depending on global properties. For instance, 2D closed surfaces are classified depending on the number of handles. In that respect, the cup of tea and the donut of figure 2 belong to the same family. The index that counts those handles is the **genus** denoted g. The genus is related to another index, the Euler characteristic of the surface Σ

$$\chi = 2(1-g) \in \mathbb{N} \tag{22}$$

If you deform the surface into a polyhedra, Euler characteristic is $\chi = V - E + F$, with V, E, F the number of vertices, edges, and faces.

Gauss-Bonnet formula. The Euler characteristic of a surface is a global, topological property. It can be related to the Gauss curvature of the same surface, which is a local, geometrical properties of the surface. At any given point of the surface, the Gauss curvature denoted K is given by the product of minimal and maximal curvatures of the surface along the set of tangent lines to at this point. Gauss-Bonnet formula relates the integral of Gaussian curvature on the whole surface to the Euler characteristic:

$$\chi = \frac{1}{2\pi}\int_{\Sigma} K d\Sigma \tag{23}$$

Deforming Σ will change the local curvatures, but not the integral! You can contemplate this relation for a long time. This is a beautiful formula, and a useful formula for the remaining of this lecture.

Topology of vector bundles. Here we will consider slightly more complicated objects than surfaces. We will look at bundles of complex normalized eigenvectors parameterized over a closed surface. To get an intuition of such objects, think first of a field of vectors tangent to a 2D closed surface as displayed figure 2c and recall hairy ball theorem: a continuous tangent vector field on a sphere necessarily vanishes at some location. One can move the singularities on the sphere by changing smoothly the vector field, but the net number of singularities is a topological invariant.By contrast, tangent vector fields on a torus are topologically trivial (one can continuously deforrms the field into a set of parallel vectors).

Counting singularities in vector fields. FIGURE. Recall that the index of a singularity at point x_i for a two dimensional vector field denoted v over a 2D base space M counts the number of revolution experienced by the vector v along a contour encircling the singularity FIGURE. Poincaré-Hopf theorem is a generalization of Hairy Ball theorem that states the net number of singularities is equal to the Euler characteristic.

$$\chi = \sum_i \mathrm{Index}_{x_i}(v) \tag{24}$$

First Chern number In the following, we will describe topological properties for a family of complex vectors denoted $\underline{\Psi}$, parameterized over a 2D closed surface. Eigenvectors of an Hermitian matrix, more precisely. As explained below in the specific case of bulk Kelvin problem, complex vector bundles parameterized over a closed manyfold exhibit same kind of singularities as bundles of real vectors. The topological invariant that counts those singularities is not anymore the Euler characteristic. It is a Chern number. More specifically, this is the first Chern number.

Phase singularities in parameter space. FIGURE. Let us go back in parameter space (k, l, f) for Kelvin bulk problem, and let us consider polar coordinates (r, θ, φ) in this parameter space. Let us look at the the eigenvector of positive frequency ($\omega_+ = r$). Their polarization relation does not depend on r:

$$\underline{\Psi}_+ = \begin{pmatrix} u_+ \\ v_+ \\ \eta_+ \end{pmatrix} = \frac{1}{r\sqrt{2}\sqrt{k^2+l^2}} \begin{pmatrix} kr + ilf \\ lr - ikf \\ k^2 + l^2 \end{pmatrix} = \frac{1}{\sqrt{2}} \begin{pmatrix} \cos\varphi - i\cos\theta\sin\varphi \\ \sin\varphi + i\cos\theta\cos\varphi \\ \sin\theta \end{pmatrix} \tag{25}$$

This mode is defined up to a phase α. In mathematical terms, this phase choice gives a section of the fiber bundle of eigenmodes. With our choice, we find two singularities: one in $\theta = 0$, another one at $\theta = \pi$. At those points eigenmodes are multivaluated and turn by an angle of 2π with φ. Another section $\tilde{\underline{\Psi}}_+ = e^{i\alpha(\theta,\varphi)}\underline{\Psi}_+$ corresponding to another phase choice allows to cancel locally those singularities, but it only moves them in the unit sphere. The impossibility to cancel globally those singularities is a topological properties of the fiber bundle, and the singularity is quantified by the first Chern number. For each band n, there is a Chern number $\mathcal{C}_n \in \mathbb{Z}$.

Q) *Derive expression 25 by computing the positive frequency eigenvector of (11), and find the expression of the two other eigenvectors. Check that eigenvectors of the flat band ($\omega_0 = 0$) correspond to geostrophic modes, and that bundles of such zero frequency eigenvectors are topologically trivial (no singularity). Hint: diagonalize first the matrix (11) in cartesian coordinates (k, l, f) and then switch to polar coordinates, with*

$$k = r\sin\theta\cos\varphi, \quad l = r\sin\theta\sin\varphi, \quad f = r\cos\theta. \tag{26}$$

Another look at phase singularities, in wavenumber space. A nice way to see the singularities of the vector bundle in each Hemisphere is to compute and plot, for a given value of f, the quantity

$$\Theta_f(k,l) = v_+(k,l)\eta_+^*(k,l) \tag{27}$$

For more details and applications to observations, go to see the posters of Wei Xuan Xu and Ziyan Zhu, and Zhu et al Arxiv 2022.

1.7 Chern number, Berry curvature and Chern-Gauss-Bonnet formula

They are several way to compute the Chern number. One is to make a phase choice, look at the singularities on the surface, to determine the winding associated with each singularity and to sum them (see Faure lectures for more detailed computations). Another may, more popular among physicists, is to use a generalization of Gauss Bonnet formula proposed by Chern himself in 1945. For this we need to introduce a quantity analogous to Gauss curvature, but suited for complex eigenmode bundles.

Berry curvature. How to quantify local twist of normalized eigenmodes $\underline{\Psi}(k,l,y)$, independently from any phase choice? By introducing the Berry curvature vector[1]

$$\mathbf{F} = (F_k, F_l, F_f) = (\mathcal{F}_{lf}, \mathcal{F}_{fk}, \mathcal{F}_{kl}) \tag{28}$$

with components

$$\mathcal{F}_{\lambda\mu} = i\left(\frac{\partial\underline{\Psi}^\dagger}{\partial\lambda}\cdot\frac{\partial\underline{\Psi}}{\partial\mu} - \frac{\partial\underline{\Psi}^\dagger}{\partial\lambda}\cdot\frac{\partial\underline{\Psi}}{\partial\mu}\right). \tag{29}$$

We have used the standard inner scalar product $\underline{\Psi}_n^\dagger \cdot \underline{\Phi} = \sum_{j=1} \underline{\Psi}_j^* \underline{\Phi}_j$ where $\underline{\Psi}_j$ is the j^{th} component of $\underline{\Psi}$.

Q) *Check that the Berry curvature does not depend on the phase choice for $\underline{\Psi}$.*
Q) *Show that the Berry curvature vector for the three wavebands of the Kelvin buk problem are*

$$\mathbf{F}_- = -\frac{\mathbf{r}}{r^3}, \quad , \mathbf{F}_0 = 0, \quad \mathbf{F}_+ = \frac{\mathbf{r}}{r^3}, \quad \mathbf{r} = \left(k, l, f\right), \tag{30}$$

[1] For those familiar with differential calculus, the Berry curvature is best interpreted as a 2-form, but such knowledge is not needed here.

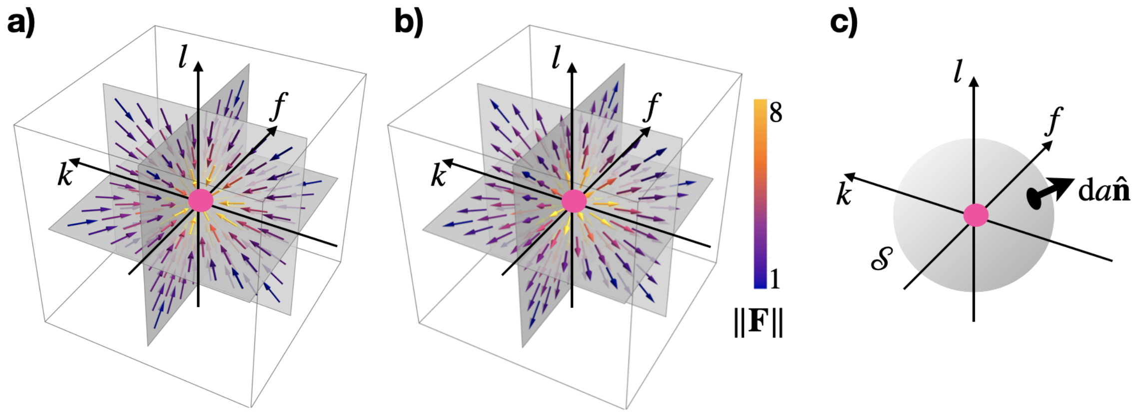

Figure 8: a) Berry curvature for the negative frequency shallow water Poincaré wave band b) same for positive frequency Poincaré wave band. c) Surface enclosing the degeneracy point to be considered to compute the first Chern numbers associated with each Berry-Chern monopole. Figure by Armand Leclerc taken from *Venaille et al arxiv 2022*

as displayed in figure 8.
Hint: for a simple (but tedious) derivation, use the expression of eigenvectors in cartesian coordinates and apply (29) . If you are familiar with 2-forms, it s more straightforward to use polar coordinates.

Chern-Gauss-Bonnet formula relates the integral of Berry curvature flux across the surface in parameter space (a geometrical quantity), to the first Chern number (a topological quantity):

$$\mathcal{C} = \frac{1}{2\pi}\int_{\Sigma} \mathbf{F}\cdot \mathrm{d}\mathbf{\Sigma} \in \mathbb{Z} \tag{31}$$

where $\mathrm{d}\mathbf{\Sigma}$ is a surface element oriented in the direction normal to the surface.

Q*) Use Chern-Gauss-Bonnet formula and expression of the Berry curvature (30) to compute the Chern numbers of eigenvector bundles parameterized over the unit sphere in (k, l, f) space for the Kelvin bulk problem:*

$$\mathcal{C}_- = -2, \quad \mathcal{C}_0 = 0, \quad \mathcal{C}_+ = +2 \tag{32}$$

Analogy with magnetic monopoles. The previous computation shows that the Berry curvature $\mathbf{F}_+$ has a form identical to a magnetic field that would be generated -by a monopole of charge 2 located at the origin in parameter space (k, l, f). We stress that the origin is peculiar as it corresponds to a degeneracy point where the three bands touch each others.

Because of this analogy, it is often said that the band-touching point carry a topological charge that generates the Berry curvature.

Q*) What would be the Chern number of inertia-gravity eigenvector bundles parameterized over a closed surface that do not enclose the origin in (k, l, f) space?*

1.8 First encounter with a bulk-interface correspondence.

Manifestation of an index theorem. Let us summarize our findings. In the first part of the lecture, we computed the dispersion relation of a bulk problem (Kelvin problem) in unbounded geometry. **We noticed the existence of three wavebands, separated by a gap.** Then we computed the spectrum of the same PDE, albeit with a coefficient $f(y)$ varying in one direction (Matsuno problem). **We noticed the existence of a spectral flow** when the wavenumber k in x direction is varied from $-\infty$ to $+\infty$, with modes transiting from one waveband to another. The number of modes gained or lost by each waveband was

$$\mathcal{N}_- = -2, \quad \mathcal{N}_0 = 0, \quad \mathcal{N}_+ = +2. \tag{33}$$

Compare with the Chern numbers of each wavebands in Eq. (32): **topological and spectral index are the same for each waveband!** This is not a coincidence. This is a manifestation of a deep mathematical result called Atiyah-Singer index theorem.

Difference with standard bulk-edge correspondence. In systems with an underlying symmetry, it possible to define a Chern number for the bulk on each side of the interface, owing to the existence of a Brillouin zone (a 2D torus in wavenumber space). The spectral flow for the system with two topological phases stacked together is then deduced from the difference of Chern number in each material. This should be contrasted with the equatorial case where the bulk Chern number describes the interface itself.

Take home message. The global shape of Matsuno dispersion relation (spectral index) could have been predicted just by computing the topological properties encoded in the eigenvectors of Kelvin problem in unbounded geometry (topological index). This is called **bulk-interface correspondence**, as it relates the spectrum of a partial differential equation (PDE) having spatially varying coefficients to topological properties of a dual matrix problem derived form the same PDE, albeit with constant coefficients. **We will see in lecture 2 a systematic way to define the "bulk problem" from the knowledge of an "interface problem" -a PDE with spatially varying coefficients.**

Qualitative interpretation. Consider a flat northern hemisphere and a flat southern Hemisphere. Their f-plane dispersion relation can not be distinguished. One could naively think that gluing together those two hemisphere would yields to the same gapped dispersion relation. However, this is not possible: in order to build eigenmodes associated to each point of the dispersion relation, assuming that f varies smoothly, one would need to continuously deform the whole family of eigenmodes parameterized in the plane k, l from a Southern hemisphere ($f < 0$) into the family of eigenmodes in the Northern hemisphere (same plane k, l for $f > 0$). This is prohibited by the presence of the Chern monopole along the way, in parameter space (k, l, f). The only way to bypass this obstruction is to close the frequency gap. This is the role played by modes that transit from one wave bands to another. This argument does not explain why the Chern number is the spectral flow index. **In lecture 3, we will use ray tracing and quantization rules to explain more precisely the bulk-interface correspondence.**

1.9 What is really "topological" in the wave spectrum?

The modes that transit from one waveband to another are often referred to as topological waves. But what is "topological" in their properties?

Robustness of the spectral flow to deformations of the profile $f(y)$. FIGURE The previous results allows to classify family of spectra for rotating shallow water equations depending on the profile $f(y)$. The classification yields predictions for the presence or absence of a spectral flow in the spectrum. If there is a single equator, the spectral flow is the same as for Matsuno beta plane computation, whatever the shape of $f(y)$.

Even if it is less relevant for geophysics, one can also make predictions for more exotic situations: the spectral flow remain the same if there is an odd number of equators. By contrast, there will be no spectral flow if the profile $f(y)$ is such that there is no equator, and more generally if there is an even number of equators.

Unidirectional. FIGURE We have seen that the f-plane system behaves as an insulator. This is a common situation in physics, when multiple fields are involved. In the presence of an interface as the equator, the gap is filled by the new topological waves. The existence of a spectral flow $\mathcal{N} = 2$ implies the existence of 2 more rightward (eastward) propagating modes that leftward (westward) propagating modes at any frequency within the frequency gap. Mode propagation refers here to the propagation of wave energy. The toplogical modes are said to be chiral as their image in a mirror is not an admissible solution. Note that because of the beta term effect, all the modes are actually chiral in Matsuno problem, but this involves only small corrections to the corresponding f-plane dispersion relation, and those modes can continuously deformed to the f-plane one by changing the profile $f(y)$, by contrast with Kelvin and Yanai waves that are

Q) *Check this property in Matsuno spectrum. Remember that energy propagation if given by group velocity, which, in the presence case is* $\partial_k \omega$.

Trapping of the modes. Kelvin and Yanai modes are more trapped than the others. In fact, all modes but those two "topological modes" become delocalized if $f(y)$ is a (sufficiently smooth) step function varying from $-f_0$ to f_0. In that case the trapping length scale is c/f_0.

Q) *Given the previous properties, think about what happens in the spectrum when* $f(y)$ *(i) is a decreasing monotonic function (ii) is a function with multiple steps and multiple equators. Hint for (ii): discuss the effect of changing the trapping length scale.* ***Use dedalus to play and make numerical experiments*** *on the spectrum of rotating shallow water model, either in a channel geometry (be careful with the effect of the walls), or in a doubly periodic geometry. FIGURE*

Equatorial waves on the sphere. The equatorial Rossby radius of deformation $\sqrt{c/\beta}$ on a planet of radius a with rotation rate Ω scales as $\sqrt{ca/\Omega}$. For a finite zonal wavenumeber k , the beta plane approximation is justified in the limit where the parameter $\sqrt{c\ \Omega a}$ vanishes, so that the planet size is much larger than the equatorial radius of deformation. The spherical case with $\sqrt{c/\Omega a}$ of order one involves several complications. Their are finite-size effects such as quantization of the zonal wavenumber, and changes in the meridional structure of eigenmodes. In addition, their are geometrical effects; for instance, Kelvin-like waves in a curved surface are dispersive.

1.10 Reading material

- To more about atmospheric and oceanic applications of Matsuno spectrum: *Vallis's book (2nd edition 2017).*
- To know more about rotating shallow water model: *Zeitlin's book (OUP 2018)*
- To know more about fiber bundles, chern number and Berry curvature: *Faure's lectures (Arxiv 2019) or Delplace's lectures (SciPost 2021) or Perez ' PhD thesis (2022)à.*
- To know more about equatorial waves in the atmosphere, see *Venaille, Dias, Cheng (preprint for encyclopedia ISTE 2023)*

2 Lecture 2: coastal Kelvin waves (1880) are topological, too.

2.1 Objectives

The main aim of today's lecture is to show to apply the topological framework introduce in lecture 1 to more complex situations. This will highlight the power of the approach, that may bypass brute force computations to obtain useful information of spectral properties of wave operators with spatially varying coefficients.

We will focus on rotating shallow water waves with varying bottom topography and ask the folllowing question:

Do the celebrated coastal Kelvin waves have a topological origin ?

The lecture will be the opportunity to discuss the qualitative consequences of discrete symmetries breaking in physical system, and, at a technical level, to introduce Wigner-Weyl transform and symbolic calculus. Those tools were born in semi-classical analysis, and are now routinely used in the physics and mathematics of fluid waves.

The same topics could have been covered in the context of plasma physics, or stratified compressible fluids. Your favorite flow model may actually also present interesting topological features that could be tackled with the approach presented in this lecture.

This lecture is based on a paper with P. Delpace published in Phys Rev Res. in 2021.

2.2 Time reversal symmetry in rotating shallow water equations

Let us recall the rotating shallow water equations on the f-plane:

$$i\frac{\partial}{\partial t}\begin{pmatrix}u'\\v'\\\eta'\end{pmatrix} = \begin{pmatrix}0 & if & -ic\frac{\partial}{\partial x}\\ -if & 0 & -ic\frac{\partial}{\partial y}\\ -ic\frac{\partial}{\partial x} & -ic\frac{\partial}{\partial y} & 0\end{pmatrix}\begin{pmatrix}u'\\v'\\\eta'\end{pmatrix}, \tag{34}$$

The multiplication by i is there for convenience as wave operators on the r.h.s. becomes Hermitian. Assuming constant f, those equations are symmetric under the transformations

$$T: \ (t,x,y,u,v,\eta,f) \ \rightarrow \ (-t,x,y,-u,-v,\eta,-f) \tag{35}$$
$$M_x: \ (t,x,y,u,v,\eta,f) \ \rightarrow \ (t,-x,y,-u,v,\eta,-f) \tag{36}$$
$$M_y: \ (t,x,y,u,v,\eta,f) \ \rightarrow \ (t,x,-y,u,-v,\eta,-f) \tag{37}$$
$$I_*: \ (t,x,y,u,v,\eta,f) \ \rightarrow \ (-t,-x,-y,u^*,v^*,\eta^*,-f) \tag{38}$$

T is the classical time-reversal symmetry, M_x and M_y are mirror symmetries. Note that isotropy is preserved, so mirror symmetry would hold in any direction. the last symmetry I_* is the complex conjugation, related to the fact that the original equation describes real fields with real coefficients; this symmetry yields to the complexe conjugate transform of the original equation. When f is prescribed, those symmetries are broken, but the combination of two of those symmetries remains a symmetry, and the combination of all symmetries plus assumption of real fields to the original set of equation (this can be interpret as a kind of CPT symmetry for shallow water flows.

Q) *Check those symmetries and provide a graphical interpretation of.*

Vocabulary across scales. Be aware that time reversal may have different meaning depending on the field you are working one (fluid dynamics, condensed matter, particle physics,...). See e.g. Delplace et al (Science 2017) and David et al (PoF 2022) for some translations in fluid context.

Why do we care about discrete symmetries? Discrete symmetries can be translated as a symmetry for the wave-operator, which put important constraints on its spectrum, as we shall see.

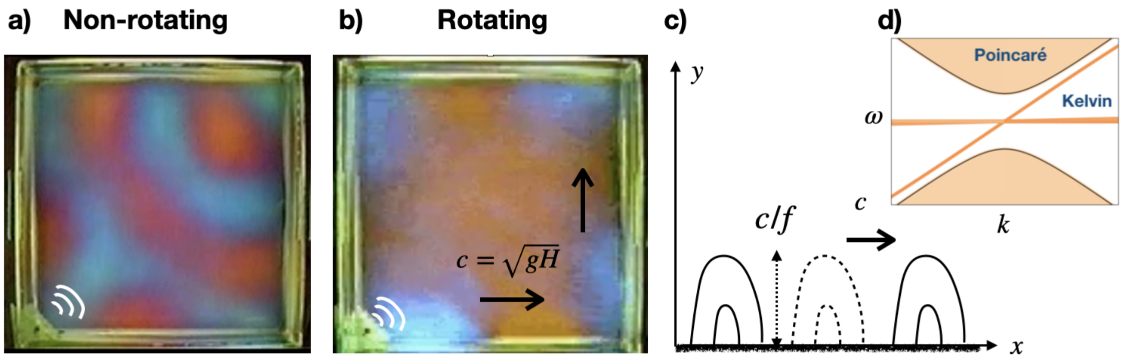

Figure 9: **a)** Shallow water waves in a non rotating tank (colors represent variations in wave amplitude), in a non rotating case: wave propagate in the bulk. **b)** Same forcing and same experimental set up, in a rotating tank. For forcing frequency between 0 and f, the only mode that can be excited is a trapped mode, the coastal Kelvin wave mode Experimental results taken from `https://www.gfd-dennou.org/library/gfd_exp/exp_e/exp/kw/index.htm`. **c)** Structure of the Kelvin wave mode in a semi-infinite domain. **d)** Dispersion relation in the semi-infinite domain case.

As far as topology is concerned, general classification have been proposed to determined wether a system may exhibit topological properties depending on broken discrete symmetries and dimension of the system. For instance, 2D systems with broken time-reversal symmetries are expected to exhibit non trivial Chern numbers, and the rotating shallow water equations belong to the same class of symmetries as 2D films of Helium 3 in phase A or p-wave superconductors.

We already saw two consequences of the presence of time-reversal symmetry breaking parameter f in shallow water equations:

- it opens a frequency gap in the dispersion relation of f-plane waves
- it leads to unidirectional modes in the β-plane configuration.

We show below two other consequences of time-reversal symmetry breaking.

- it leads to unidirectional modes along coasts.
- it leads to phase singularities in eigenmode structures.

2.3 First consequence: unidirectional trapped modes along coasts

So far we considered unbounded geometries. Motivated by the study of dynamical tides in Earth ocean, Kelvin looked at the effect of an impermeable wall (a sharp coast, say for instance on the $y = 0$) on the f-plane wave spectrum. In addition to the bulk modes, he found an unidirectional wave branch, with

$$\omega = ck, \quad u = \eta = Ae^{-yf/c}, \quad v = 0. \tag{39}$$

This wave is similar to the equatorial Kelvin wave of previous lecture. The mode is exponentially trapped at the wall over a scale c/f. The coastal Kelvin wave mode structure in this simple configuration and the corresponding dispersion relation is displayed figure 9. For more complex boundary shapes, this wave still exists. It moves cyclonically along the coast, at the speed of non-rotating shallow water waves. Look for instance at movies of tidal motion in the ocean. You will notice trapped modes along South America, or along the coast of sufficiently large bays and lake, or closed seas. Those are coastal Kelvin mode (although the tidal response involves a superposition with other modes). Those modes can also be observed in laboratory experiment, as shown figure 9a,b, and as discussed in the appendix of lecture 1.

Q) *Compute the fulll spectrum of shallow water waves on a semi-infinite plane, by imposing the impermeability constraint $v = 0$ at $y = 0$. Show the existence of a wave branch $\omega = ck$ that is*

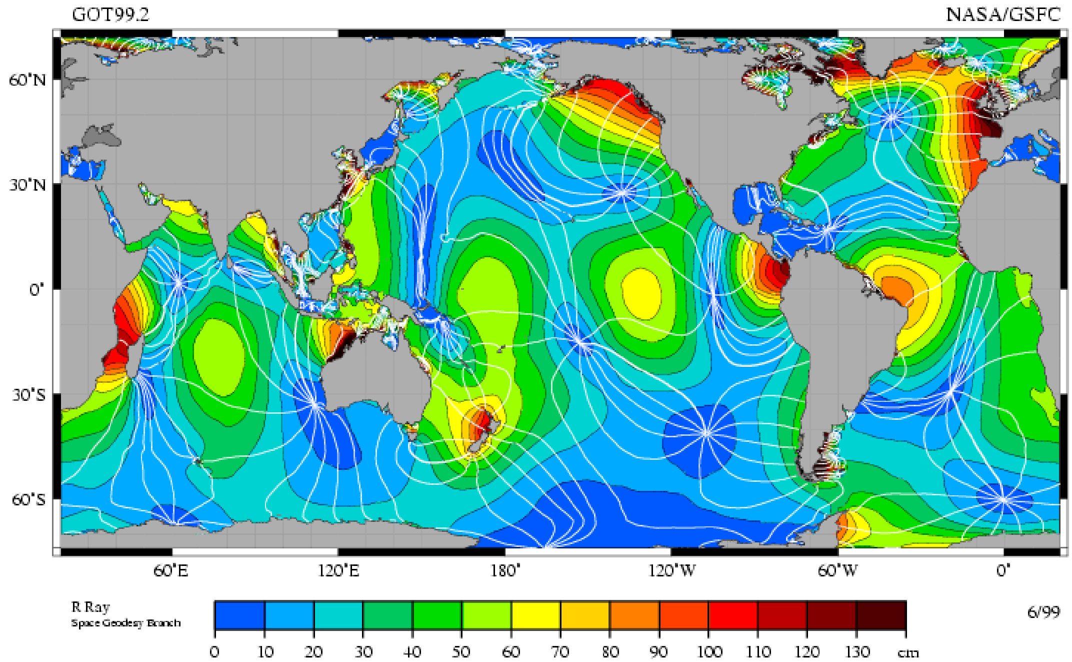

Figure 10: Structure of ocean tides in response to gravitational attraction of the Moon (M2 tide). The color gives tidal amplitude. Cotidal lines are displayed in white. Along a white line, high tide or low tide occurs at the same time. Note the presence of amphidromic points where cotidal lines meet and amplitude vanishes. This is the first example of a phase singularity found in a physical system.

at geostrophic equilibrium in the y-direction only. Why is the solution $\omega = -ck$ forbidden?

This is arguably the first example of an unidirectional trapped mode in physics. The aim of today's lecture is to show the topological origin of such waves.

Why is this important? A result from topology would explain the existence of coastal Kelvin in a much wider class of configurations (including complicated coastlines), and explains its robustness against disorder (remember that you see this waves on realistic simulations or observations).

Why it is challenging? in the problem posed by Kelvin (f-plane on a flat bottom), there is no way to extract a Chern number. Remember that to define a Chern number you need a vector bundle over a closed surface. One could identify the plane (k,l) to a sphere, but this is not possible in the shallow water casse as the vector field at infinity can not be identify to a single point. A regularization parameter (such as odd viscosity) can be added to fix this issue, but this change the order of the equation. Another possibility, followed in this lecture, is to interpret the hard wall configuration as a limiting case of a varying bottom topography (which is actually more realistic to describe actual coasts !). *See two papers by Tauber et al 2019, 2020, for more discussions and a paper by Parker et al 2020 for a plasma example where the plane (k,l) can be identified to a sphere.*

2.4 Second consequence: amphidromic points in tidal waves.

Before addressing the topological origin of Kelvin waves, it is worth looking at another consequence of time-reversal symmetry in bounded ocean demain: the change of topology in the spatial structures of the eigenmodes, with the appearance of phase singularities.

We already encountered an example of phase singularities in lecture 1, but in parameter space, which is nicely illustrated by plotting the crosscorrelation $v(k,l)\eta^*(k,l)$ for a given value of $f \neq 0$

(see Zhu et al preprint). In addition, we explained that this singularity is related to the presence of Berry-Chern monopole in parameter, that reflects the impossibility to define continuously the phase of eigenvectors parameterized over the surface enclosing this monopole. Here we show a spectacular manifestation of phase singularities in physical space: the amphidromic points discovered by sea-going oceanographers when drawing tidal maps in XIX century.

Consider and eigenmode of the shallow water system in a closed domain, with frequency ω. The sea surface elevation of this eigenmode can be writen as

$$\eta(x,y,t) = \hat{\eta} e^{i\omega t} + \hat{\eta}^* e^{-i\omega t}, \quad \hat{\eta}(x,y) \in \mathbb{C} \tag{40}$$

When $f = 0$, time reversal symmetry of the solution implies $\eta(x,y,t) = \eta(x,y,-t)$, and hence $\hat{\eta} = \hat{\eta}^*$: the amplitude $\hat{\eta}(x,y)$ is real. Real functions of two variables vanish generically along lines. Thus, the amplitude of the sea surface height vanishes along lines in the horizontal plane in that case. This corresponds to seiche modes (think of a stationary wave in a small tank).

When $f \neq 0$, time reversal symmetry is broken, and $\hat{\eta} \neq \hat{\eta}^*$: the field $\hat{\eta}$ is a complex field. This field generally vanishes at isolated points in the 2D plane (both the real part and the imaginary part are real functions of two variables that cancel along lines; the field $\hat{\eta}$ vanishes at the intersections between those lines). Those isolated points correspond to phase singularities known as amphidromic points displayed figure 10.

Amphidromic points are arguably the first example of a **phase singularity** in physics. As noticed by M. Berry, two other types of singularities are encountered in the physics of waves: (i) **singularities the intensity**, or of the amplitude, as caustics, which happens generically in fluid context when considering waves propagation with a background mean flow, as bundle of ray trajectories may then converge to a critical line where wave phase speed equal mean flow velocities; (ii) **singularities of the polarization relation**, that correspond to the band degeneracy points that we described in previous lectures, and that are characterized by a Berry-Chern monopole.

This subsection is adapted from Berry's papers "Quantum chaology" (Proc Roy Soc 1985), and "Making waves in physics" (Nature 2000). See also Perez PhD thesis (2022, ENS de Lyon) who gives other example of phase singularities in hydrodynamics.

2.5 Shallow water with varying bottom topography

Just as we interpreted equatorial shallow water wave spectrum as an interface problem with a dual bulk problem admitting non trivial topological properties, we propose now to interpret the coastal problem as an interface problem.

An impermeable wall at $y = 0$ is the limiting case of a continental shelf where the fluid depth tends to $H = 0$ at $y = 0$. We thus now consider shallow water dynamics with variable bottom topography $H(y)$. The linearized dynamics around a state of rest is described by

$$\partial_t \begin{pmatrix} u \\ v \\ \eta \end{pmatrix} = \begin{pmatrix} 0 & f & -g\partial_x \\ -f & 0 & -g\partial_y \\ -\partial_x(H\cdot) & -\partial_y(H\cdot) & 0 \end{pmatrix} \begin{pmatrix} u \\ v \\ \eta \end{pmatrix} \tag{41}$$

This system conserves energy

$$E = \frac{1}{2} \int \left(Hu^2 + Hv^2 + g\eta^2 \right) dxdy \tag{42}$$

It is convenient to rescale the problem as follows:

$$i\partial_t \underline{\Psi} = \mathcal{H}_{op} \underline{\Psi}, \quad \underline{\Psi} \equiv (\sqrt{H}u, \sqrt{H}v, \sqrt{g}\eta)^t \tag{43}$$

$$\mathcal{H}_{op} \equiv i \begin{pmatrix} 0 & f & -c\partial_x \\ -f & 0 & -c\partial_y \\ -c\partial_x & -c\partial_y - 2\beta_t & 0 \end{pmatrix} \tag{44}$$

where we have introduced the y-dependent wave phase speed and a new parameter, the relative gradient of bottom topography

$$c \equiv \sqrt{gH}, \quad \beta_t \equiv \frac{1}{4} c \frac{\partial_y H}{H} \ . \tag{45}$$

Q) *To see the interest of this rescaling, check that energy conservation in the rescaled system is expressed as the conservation of the norm for $\underline{\Psi}$ with standard scalar product. This is useful because topology deals with normalized eigenvectors.*

The coast. We now consider the case of a profile $H(y)$ that increases from 0 (the coastline) to a constant depth at large y (the ocean interior). The corresponding profile β_t decreases from $+\infty$ to 0 as y increases. This is the interface problem of this lecture. But where is the interface? And, what is the corresponding bulk problem?

2.6 The bulk: symbols and Wigner-Weyl transforms

In lecture 1, we noticed that important information on the spectral properties of an operator with spatially varying coefficients (interface problem, Matsuno) are encoded in a topological invariant of a dual matrix problem involving constant coefficient (bulk problem, Kelvin). How to define systematically this dual bulk matrix problem, for a given operator?

Symbol of an operator. In the case of equatorial waves, the matrix of the bulk problem denoted $\underline{\underline{H}}_k(y, l)$ can be deduced from the Matsuno operator $\hat{\underline{\underline{\mathcal{H}}}}_k(y, \partial_y)$ by assuming that y is a parameter and by identifying $-i\partial_y$ with the wavenumber l. In mathematical term, this procedure amounts to compute the symbol of an operator. Symbols are functions of position and wavenumbers, that can either be scalars, vectors, or matrices. Here we are interested in multicomponent wave problems that involve symbol matrices.

Wigner-Weyl transforms. A systematic way to compute a symbol $g(y, l)$from the knowledge of an operator $\hat{g}(y, \partial_y)$ is to use a Wigner transform, and the reverse procedure is called Weyl quantization. All we will need for our purpose can be derived from the definition of the Weyl transform:

$$\hat{g}\psi(y, t) = \frac{1}{2\pi} \int \mathrm{d}y' \mathrm{d}l \ e^{il(y-y')} g\left(\frac{y+y'}{2}, l\right) \psi(y') \tag{46}$$

Q) *Check the following correspondence between symbols and operators:*

$$\text{Symbol} \quad \leftrightarrow \quad \text{Operator} \tag{47}$$
$$g \quad \leftrightarrow \quad \hat{g} \tag{48}$$
$$l \quad \leftrightarrow \quad -i\partial_y \tag{49}$$
$$c(y) \quad \leftrightarrow \quad c(y) \tag{50}$$
$$c(y)l \quad \leftrightarrow \quad -ic(y)\partial_y + \frac{c'(y)}{2} \tag{51}$$

The last line is essential: products of operators are different than operator of symbol products. We will come back to this point in the third lecture.

Historically, such quantization procedures were devised to derive operators of quantum mechanics from the knowledge of classical dynamics in phase space (y, l), with the energy $e(y, l)$ playing the role of the symbol. Among the different existing quantization procedure, Weyl transform plays a particular role as it translate the hermiticity of the operator at the level of the symbol.

Q) *Check that the symbol of the coastal wave operator (44) is indeed an hermitian matrix:*

$$H_{\text{bulk}} \equiv \begin{pmatrix} 0 & if & ck \\ -f & 0 & cl + i\beta_t \\ ck & cl - i\beta_t & 0 \end{pmatrix} \tag{52}$$

We can now apply the same strategy as for equatorial waves: study topological properties of the bulk problem (symbol) and then use this knowledge to interpret spectral properties of the corresponding operator with spatially varying coefficients. Here f will be fixed, and $\beta_t(y)$ will be varied.

2.7 A fluid analogue of Haldane's model

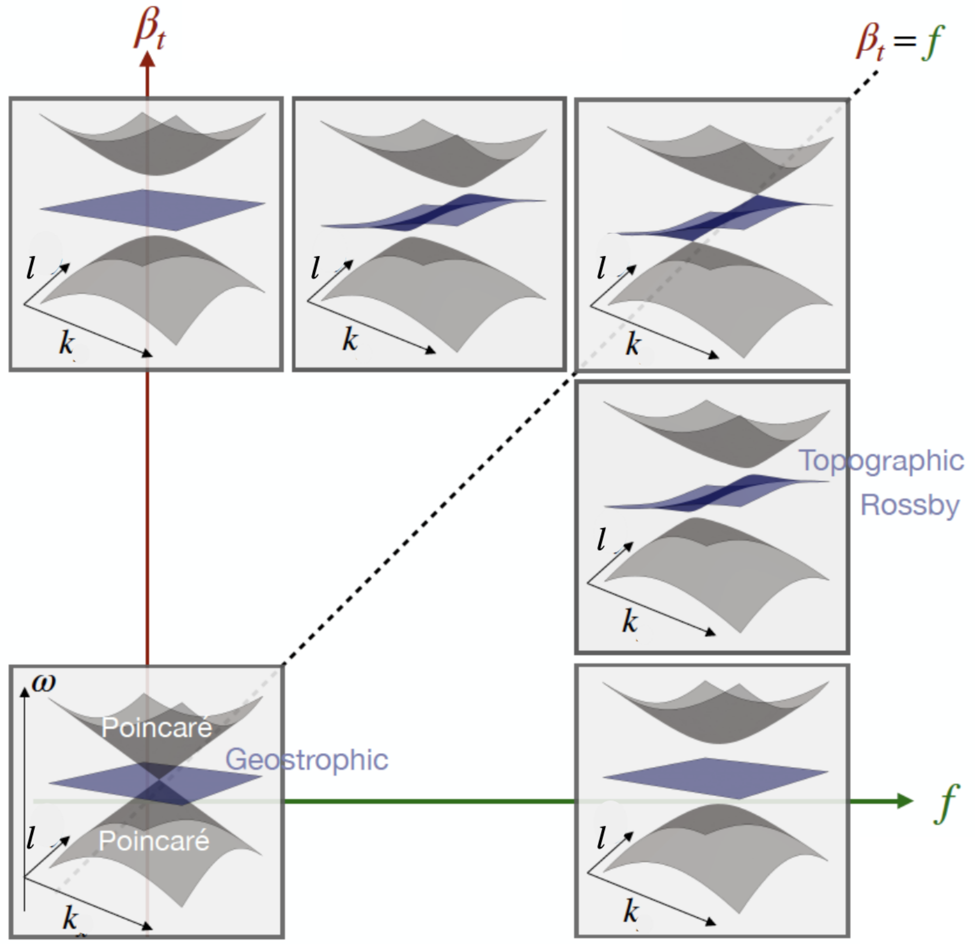

Figure 11: Dispersion relation for the bulk problem of rotating shallow water waves with bottom topography, found by solving (55). *Figure by Pierre Delplace, adapted from Venaille and Delplace PRR 2021.*

We now describe topological properties of the symbol for coastal waves. The strategy is to identify band-touching points, and to compute the Chern numbers associated with them, just as in the equatorial case. Before this, another remark on discrete symmetry, the theme of this second lecture:

Discrete symmetries. The operator (44) is left invariant under the transformations

$$T: \ (t, x, y, u, v, \eta, f, \beta_t) \ \rightarrow \ (-t, x, y, -u, -v, \eta, -f, \beta_t) \tag{53}$$

$$M_y: \ (t, x, y, u, v, \eta, f, \beta_t) \ \rightarrow \ (t, x, -y, t, u, -v, \eta, -f, -\beta_t) \tag{54}$$

We see that the new parameter β_t in Eq. (52) breaks mirror symmetry in the y direction without breaking time-reversal symmetry. Thus, we get a physical problem featuring a parameter f breaking time-reversal and mirror symmetry, together with a parameter β_t breaking mirror symmetry only. This is reminiscent of Haldanes's model in condensed matter.

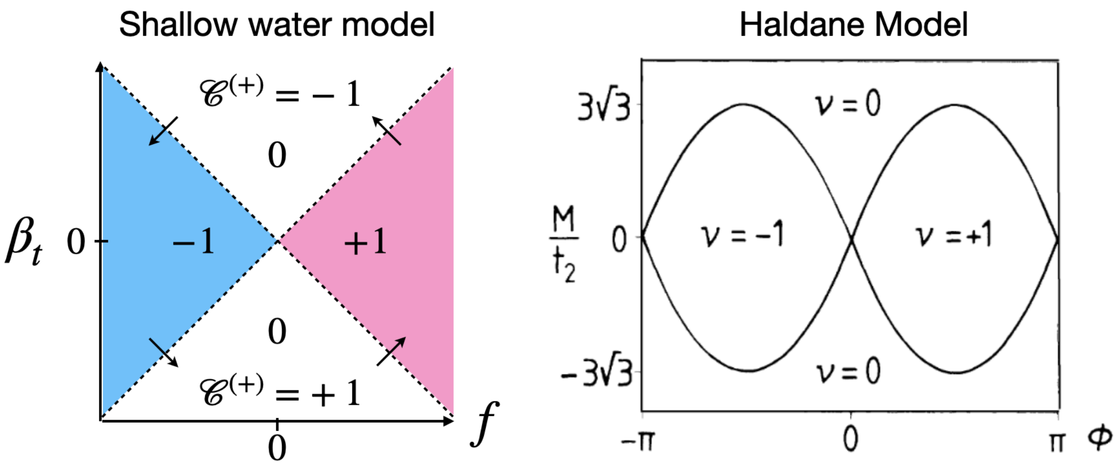

Figure 12: **Analogy between the bulk version of rotating shallow water model with varying bottom topography and Haldane model.** Coriolis parameter f and topographic gradient β_t play the same role as ϕ and $M//t_2$ in Haldane model in the limit where those two Haldane parameters are small. In Haldane model the index in each phase are Chern numbers. In shallow water model, the value of the Chern number $\mathcal{C}^{(+)}$ of the upper wave band is -1 along $\beta_t = f$ and $\mathcal{C}^{(+)} = 1$ along $\beta_t = -f$. Those Chern numbers are recovered by taking the difference of the index given in each parameter region. *The left figure is adapted from N. Perez PhD thesis 2022. The right figure is taken from original Haldane paper PRL 1988.*

Dispersion relation. The eigenvalues ω of the matrix (52) are solutions of

$$\omega^3 - \omega \left(c^2k^2 + c^2l^2 + f^2 + \beta_t^2\right) + 2f\beta_t ck = 0 \ . \tag{55}$$

Solutions are displayed figure 11. We see that f and β_t play a symmetric role in the dispersion relation. In particular, β_t "opens" a frequency gap, just as f did in the Kelvin wave problem. Note also that the presence of the term β_t with $f \neq 0$ lift the degeneracy of the flat band. This corresponds to topographic Rossby waves (owing their existence to gradient of topography rather than to gradient of Coriolis parameter).

Two-fold degeneracy points. For given couple of value of $f \neq 0$, we find a two-fold degenerate eigenstates

$$l = 0, \quad \text{and } c^2k^2 = \beta_t^2 = f^2. \tag{56}$$

These lines intersect each others at the origin $(k_y, k_x, f, \beta_t) = (0, 0, 0, 0)$. This intersection corresponds to the three-fold waveband crossing point described in lecture 1. In that respect, considering the new mirror symmetry breaking parameter has lifted a single three-fold degeneracy point into two two-fold degeneracy points. At the critical value $|\beta_t| = |f|$, the topographic Rossby band touches the Poincaré band, leading to a two-fold degeneracy point around which the dispersion relation is linear (conical), as seen figure 11. Near those degeneracy points, the symmetry M_y is restored .

On the Chern number for two-folds degeneracy points. We explain in the next subsection that the Chern numbers of a two-fold band degeneracy points is either 1 or -1 (see appendix). If you pick up the correct sign for one of them, you can get all of them by symmetry. The correct initial sign can be found by a brute force computation (difficult in the present case), by a numerical computation, or, why not, by using the index theorem in a reverse way. We will come back on this point later.

Similarity with Haldane's model. Our analysis of the bulk problem for rotating shallow water waves with varying bottom topography bears strong similarities with the celebrated Haldane model that that has played a central role in the understanding of topological phases of matter:

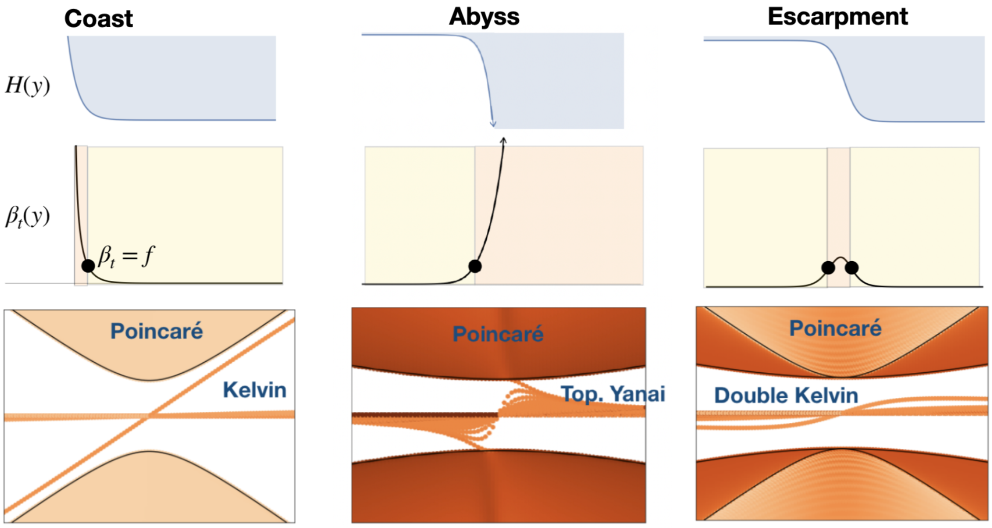

Figure 13: Spectrum of rotating shallow water waves for different bottom topography profiles. Use the profile of $\beta_t(y)$ to interpret the spectral flow in all three cases. Note that the last case (escarpment) can be thought as the concatenation of the two other cases. Use dedalus to see how those spectra are changed when $\beta_t(y)$ is continuously deformed.

`https://topocondmat.org/w4_haldane/haldane_model.html`
Haldane starting point was a conic dispersion relation for electronic waves in a toy model for graphene. As far as the dispersion relation is concerned, Haldane observed that the addition of a time-reversal symmetry breaking parameter such as f or of a mirror-symmetry parameter such as β_t in the problem would have the same effect: to open a frequency gap. By contrast, at the level of the eigenmodes, the symmetry breaking parameters f and β_t have drastically distinct effects: while non-trivial topological properties emerge in parameter (k, l, f) (see lecture 1), a similar computation in parameter space (k, l, β_t) would lead to three topologically trivial wavebands (the Chern number of the degeneracy point at the origin is zero for all wavebands). The upshot is that time-reversal symmetry must be broken to get non-trivial topological properties in this class of models.

Difference with Haldane's model. Haldane obtained a topological phase diagram displayed figure 12 by computing a Chern number for each set of bulk paramater, taking advantage that the 2D wavenumber in lattice geometry are represented on a torus (Brillouin zone). An important difference between shallow water model and Haldane model is that in the shallow water case the (f, β_t) diagram is not a topological phase diagram as one can not assign a bulk Chern number at each point (f, β_t): the topological aspect of our continuous model is expressed with a Chern number $\mathcal{C}$ obtained by considering a variation of either f or β_t around a band crossing point, that occurs at $f = \beta_t$. One can still assign an index to each regions, such that the interface Chern numbers are recovered by computing the index difference between adjacent regions, as displayed figure 12.

The upshot is that rotating shallow water waves with varying bottom topography is a fluid analogue of the central region of topological phase diagram in Haldane model.

2.8 The interface: topological origin of coastal Kelvin wave.

Where is the interface? FIGURE. Let us come back to our coastal problem: $\beta_t(y)$ is a decreasing function from $+\infty$ to 0 as y increases. This function goes through a critical latitude y_c such that a degeneracy point exists for bulk waves in (k, l, β_t)-plane. More precisely, two degeneracy points are crossed at $\beta_c(y_c) = f$: one is located at $k = -f/c$ and involves band touching between the lower and middle frequency band; a second one located at $k = f/c$ involves the middle frequency band and the upper frequency wave band (see figure). The line $y = y_c$ is the interface we were looking for. The Chern number of those two degeneracy points are the same (and this can be recovered by symmetry arguments).

Bulk-interface correspondence According to the bulk-interface correspondence, the existence of degeneracy points between bands with non trivial topological properties for the bulk eigenmodes in parameter space (k, l, β_t) manifests itself in the interface wave problem as a spectral flow: the number of modes that transit from the upper band to the lower band near any degeneracy points $k = \pm f/c$, is (algebraically) equal to the monopole Chern number $\mathcal{C}^+$ associated with those degeneracy points, up to a sign given by the sign of $\mathrm{d}\beta_t/\mathrm{d}y$. The whole shape of the dispersion relation is obtained by continuity of the wave branches.

Hard wall as a limiting case of an interface FIGURE. One can check that the hard wall case is recovered at finite k in the spectrum, for an exponential confinement of the coastal area, in the limit of vanishing e-folding distance from the coast to the bulk of the ocean.

Trapping length scale The state that transits from one band to another is trapped close to the critical value y_c where the value of β_t reaches the degeneracy point. The trapping length scale is generally given by an intrinsic length of the problem, which, in the present case, is the Rossby radius of deformation c/f.

Q) *Think of other physically interesting topography profiles (e.g. the transition from a shallow see to a deep ocean), and use the previous analysis to predict the existence of trapped modes transiting from one waveband to another. What kind of topography profile do invert the sign of the spectral flow? Are topographic bump (escarpments) topologically trivial? Can topology still be used to interpret the observed spectrum? Test those ideas using dedalus. Hint: see figure 13 and Venaille and Deplace PRR 2021.*

2.9 Reading material

- The classic (short and surprisingly modern in its notations) paper by *Thomson (Kelvin) 1880* is worth reading.
- The book by *Zeitlin 2018* gives a nice overview of coastal wave theory.
- Weyl calculus with application to shallow water waves is well introduced in *Onuki 2020 Journal of fluid mechanics* or *Faure lectures (Arxiv 2019).*
- Two band crossing points and related spectral flows are discussed in more detailed in *Delplace lecture notes (Scipost 2022)* and *Faure lecture notes (Arxiv 2019).*
- A large part of this chapter is taken from *Venaille and Delplace (PRR 2021).*

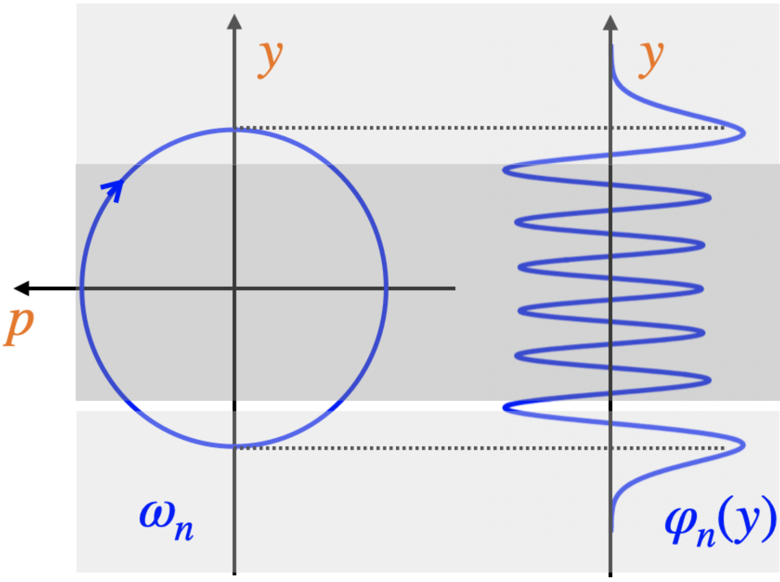

Figure 14: Relation between the eigenmode $\varphi_n(y)$ of a scalar operator $\hat{\Omega}$ and ray trajectory $\Omega(y,p) = \omega_n$. The dark grey region is where WKB ansatz applies.

3 Lecture 3: bulk-interface correspondence interpreted by ray tracing

3.1 Objectives

In lecture 1 and 2, we invoked an abstract bulk-interface correspondence based on index (Atiyah-Singer) theorems. The aim of this lecture is to get some intuition on the physical origin of this correspondence. We will illustrate the main ideas with the now familiar shallow water model on the beta plane.

This will be the opportunity to introduce tools from semi-classical analysis (WKB methods) that bridge a gap between between ray tracing in phase space and spectral properties of operators, and that can be used for many wave problems, independently from topology.

Along the way, we will show a physical manifestation of Berry curvature in ray tracing. In lecture 1, this curvature was just a mathemtical trick to compute topological properties. In this lecture we will see that it actually deflects ray trajectories.

This lecture is based on a preprint (Venaille et al, Arxiv July 2022) that revisits in the context of topological waves a classical work by Littlejohn and Flynn (PRA 1991) on ray tracing in continuous media.

3.2 Informal introduction to ray tracing and quantization condition

Let us first sacrifice rigor to illustrate informally the correspondence between ray tracing and spectral properties in a simple scalar case, the 1D quantum harmonic oscillator encountered in lecture 1:

$$i\epsilon\partial_t\psi = \hat{\Omega}\psi, \quad \hat{\Omega} = y^2 - \epsilon^2\partial_{yy} \tag{57}$$

We look for a solution $\psi(y,t)$ in the semi-classical limit $\epsilon \to 0$. Solutions can be written on the form:

$$\psi(y,t) = a(y,t)\exp\left(i\frac{\phi(y,t)}{\epsilon}\right), \tag{58}$$

In the semi-classical (WKB) framework, a, ϕ and their derivatives are of order one. A careful WKB treatment of the problem involves multiple asymptotic expansion of those fields with parameter ϵ. See the book of *Bender and Orszag* for details.

Ray trajectories in phase space. We define

$$p = \partial_y \phi \quad \omega = -\partial_t \phi. \tag{59}$$

At leading order in ϵ, (57) leads to a local dispersion relation obtained informally by assuming that spatially varying coefficients are held constant. As in lecture 2, this is done properly by computing the symbol $\Omega(y,p)$ of $\hat{\Omega}$, and the WKB expansion applied to (57) leads then to

$$\omega = \Omega(y,p), \quad \Omega(y,p) = y^2 + p^2. \tag{60}$$

This equation, together with (59), is the equivalent to Hamilton Jacobi equation in classical mechanics, with (y,p) the phase space coordinates and ϕ the action. After standard manipulations, one can deduce the Hamilton form of ray tracing equations:

$$\frac{dy}{dt} = +\frac{\partial \Omega}{\partial p}, \quad \frac{dp}{dt} = -\frac{\partial \Omega}{\partial y}, \tag{61}$$

where $(y(t), p(t))$ are now interpreted as the trajectory of a localized wavepacket in phase space FIGURE.

From rays to eigenmodes. The standard semi-classical procedure to find eigenmodes of $\hat{\Omega}$ with eigenvalue ω is to look for closed orbits $\omega = \Omega(y,p)$ in phase space and to select those orbits such that the phase ϕ/ϵ gained by the wave after a period (in phase space) is an integer multiple of 2π, to ensure that the WKB ansatz is single valued. Special care must be taken at the turning point ($p = 0$) where the WKB ansatz fails. This failure can be healed by patching the solution with another ansatz at the turning points, combined with a matching procedure. The outcome of this matching procedure is that the wave picks-up a phase $\pi/2$ at each of the turning point. This leads eventually to the Bohr-Sommerfeld quantization condition:

$$\frac{1}{\epsilon} \oint_{\omega=\Omega(y,p)} p(y)dy + \pi = 2\pi n, \quad n \in \mathbb{N}. \tag{62}$$

Where the contour is taken clockwise. The condition (62) is extremely useful as it allows to obtain information on the eigenvalues ω without solving for the eigenfunctions. In the quantum harmonic oscillator case, we recover

$$\omega = 2\epsilon \left(n + \frac{1}{2} \right) \tag{63}$$

which is actually the exact expression for the eigenvalues of $\hat{\Omega}$, whatever the value of ϵ. In more general cases, this procedure only yields to an approximate solution that is valid in the semi-classical limit $\epsilon \to 0$.

Our aim now is to generalize this approach to multicomponent wave problems, and to use it as a way to interpret the index theorem encountered in previous lectures.

3.3 A semi-classical limit for equatorial shallow water waves

Our starting point is the Matsuno wave problem described in lecture 1, written now formally as a Schrödinger-like equation:

$$i\frac{\partial}{\partial \tilde{t}} \underline{\Psi} = \underline{\underline{\hat{\mathcal{H}}}}_k \underline{\Psi} \tag{64}$$

with

$$\underline{\underline{\hat{\mathcal{H}}}}_k = \begin{pmatrix} 0 & i\tilde{y} & k \\ -i\tilde{y} & 0 & -i\frac{\partial}{\partial \tilde{y}} \\ k & -i\frac{\partial}{\partial \tilde{y}} & 0 \end{pmatrix}, \quad \underline{\Psi} = \begin{pmatrix} u \\ v \\ \eta \end{pmatrix}. \tag{65}$$

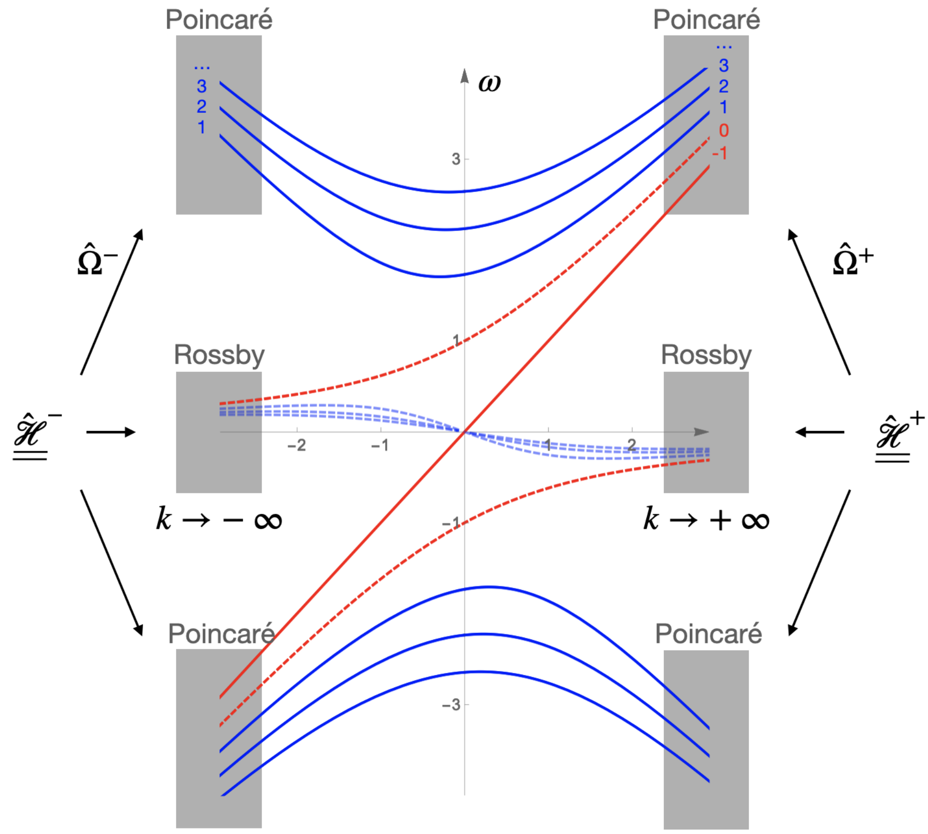

Figure 15: The aim in this lecture is to compare the number of modes on each side of each wave band, in the semi classical limits depicted as grey boxes.

Our aim is to interpret/explain the bulk-edge correspondence that predicts a spectral flow $\mathcal{N} = 2$ for the spectrum of this operator, as k is varied from $-\infty$ to $+\infty$. To show how the formula $\mathcal{N} = \mathcal{C}$ emerge, we will use ray tracing and quantization conditions in limiting cases $k \to \pm\infty$.

In the limit $k \to \pm\infty$, it is convenient to rescale the wave equation as follows:

$$(t, y) = \sqrt{\epsilon}(\tilde{t}, \tilde{y}), \quad \epsilon = \frac{1}{k^2} \tag{66}$$

which leads to

$$i\epsilon \frac{\partial}{\partial t} \underline{\Psi} = \underline{\underline{\hat{\mathcal{H}}}}^{\pm} \underline{\Psi}, \quad \underline{\underline{\hat{\mathcal{H}}}}^{\pm} = \begin{pmatrix} 0 & iy & \pm 1 \\ -iy & 0 & -i\epsilon \frac{\partial}{\partial y} \\ \pm 1 & -i\epsilon \frac{\partial}{\partial y} & 0 \end{pmatrix}. \tag{67}$$

The parameter ϵ appears only in front of the y-derivative, which is suggestive of the Planck constant $\hbar$ in quantum mechanics. This is why the limit $\epsilon \to 0$ will from now on be referred to as a **semi-classical limit**, and ϵ will be called the **semi-classical parameter**[2]. The upper-script index $\pm$ are used to distinguish the limit $k \to +\infty$ from the limit $k \to -\infty$. An important remark follows:

Understanding the spectral flow can be tackled by comparing the spectral properties of the operators $\underline{\underline{\hat{\mathcal{H}}}}^{+}$ *and* $\underline{\underline{\hat{\mathcal{H}}}}^{-}$ *in the semi-classical limit* $\epsilon \to 0$*, depicted as grey rectangles in figure* **??**. *More precisely, we will pair together modes of the two operators that share common properties. By continuity of the eigenvalues, the modes that can not be paired will be those belonging to a branch that transits from one wave band to another as* k *varies.*

[2]The name WKB parameter can also be used, but this terminology is sometimes kept for a specific class of scalar equations.

3.4 Projection of multicomponent wave operators into scalar operators

Notation In this section, we have dropped the upperscript $\pm$ that should be present to all operators and symbols to be consistent with previous subsection.

In the semi-classical limit, the wavebands are well separated from each other. The aim of this section is to write in this limit the multicomponent spectral problem as three decoupled scalar wave equations, one for each waveband. We will focus in this lecture on the positive frequency inertia-gravity (Poincaré) waveband FIGURE. Formally, we assume that the wave dynamics for this waveband can be written as

$$i\epsilon\partial_t\psi = \hat{\Omega}\psi, \tag{68}$$

with ψ a scalar field and $\hat{\Omega}$ an operator[3]. We also assume the existence of a reconstruction multicomponent operator $\underline{\hat{\chi}}$ (a vector whose each component is an operator), such that

$$\underline{\Psi} = \underline{\hat{\chi}}\psi, \quad \underline{\hat{\chi}}^\dagger \cdot \underline{\hat{\chi}} = \mathbb{1}, \tag{69}$$

where $\mathbb{1}$ is the identity operator, and where $\underline{\Psi}$ is a solution of (67). The second equality guarantees that both $\underline{\Psi}$ and ψ are normalized in the same way:

$$\int \mathrm{d}y \ \underline{\Psi}^\dagger \cdot \underline{\Psi} = \int \mathrm{d}y \ \psi^*\psi. \tag{70}$$

In the case of shallow water wave, this norm represents the total energy of the flow, which always be set to 1.

At this stage the operators $\hat{\Omega}$ and $\underline{\hat{\chi}}^\pm$ are not known. A useful equation relating those operators is obtained by combining (64), (68), and (69):

$$\underline{\underline{\hat{\mathcal{H}}}}\underline{\hat{\chi}} = \underline{\hat{\chi}}\hat{\Omega}. \tag{71}$$

Our aim now is to use this expression and **symbolic calculus** introduced in lecture 2 to find the expression of the scalar operator $\hat{\Omega}$ in the semi-classical limit.

Asymptotic expansion of the operators Formally, all the operators in (71) can be expanded as

$$\underline{\underline{\hat{\mathcal{H}}}} = \underline{\underline{\hat{\mathcal{H}}}}_0 + \epsilon\underline{\underline{\hat{\mathcal{H}}}}_1 + \mathcal{O}(\epsilon^2), \tag{72}$$

$$\underline{\hat{\chi}} = \underline{\hat{\chi}}_0 + \epsilon\underline{\hat{\chi}}_1 + \mathcal{O}(\epsilon^2), \tag{73}$$

$$\hat{\Omega} = \hat{\Omega}_0 + \epsilon\hat{\Omega}_1 + \mathcal{O}(\epsilon^2). \tag{74}$$

The same expansion is used for symbols (just remove the hat). Our aim is to obtain a formal expression of the operators by computing first their symbols in the semi classical limit, and then by using a Weyl transform.

Weyl transform and WKB limit. In order to exploit equality (71) to find expressions of $\underline{\chi}_0$, Ω_0 and Ω_1, we need to compute the symbol of the product of operator. Before this, let us write again the definition of the Weyl transform,

$$\hat{g}\psi(y,t) = \frac{1}{2\pi\epsilon}\int \mathrm{d}y'\mathrm{d}p \ e^{i\frac{p}{\epsilon}(y-y')} g\left(\frac{y+y'}{2}, p\right)\psi(y'). \tag{75}$$

This is the same definition as in lecture 2, albeit with a rescaling of the wavenumber in y direction now denoted p. We assume $p \sim 1$ and take advantage of the limit $\epsilon \to 0$ to obtain useful identities between operators and symbols in the semi-classical limit.

[3] A pseudo-differential operator, as we shall see later.

Products. We already noticed that products of operators $\hat{a}\hat{b}$ are in general different from the operator $\widehat{ab}$ obtained by a Weyl transform of the standard product between symbols $a(y,p)$ and $b(y,p)$. A useful formula relating those two products in the semi-classical limit is

$$\hat{a}\hat{b} = \widehat{ab} + \frac{i}{2}\epsilon\widehat{\{a,b\}} + \mathcal{O}\left(\epsilon^2\right) \tag{76}$$

where we have introduced the **Poisson bracket**

$$\{a,b\} = \partial_y a \partial_p b - \partial_p a \partial_y b. \tag{77}$$

Using this product rule, together with the asymptotic expansions of symbols introduced above, we can now collect terms at different order in (71).

Q) *Derive equation (76). See Appendix on Weyl-Wigner calculus for details.*

Order 0 At the lowest order, we obtain a matrix eigenvalue problem for $\underline{\underline{\mathcal{H}}}_0$:

$$\underline{\underline{\mathcal{H}}}_0 \underline{\chi}_0 = \Omega_0 \underline{\chi}_0, \quad \underline{\chi}_0^\dagger \underline{\chi}_0 = 1. \tag{78}$$

We see that symbols Ω_0 and $\underline{\chi}_0$ are just the eigenvalue and the eigenvector of the leading order wave operator symbol $\underline{\underline{\mathcal{H}}}_0$. This result may be understood as the outcome of a "local" plane wave solution: $\underline{\chi}_0$ is the local polarization vector associated with the local dispersion relation $\Omega_0(y,p)$.

Order 1 Collecting the first order terms in (71), multiplying on the left by $\underline{\chi}_0^\dagger$, and using $\underline{\chi}_0^\dagger \underline{\underline{\mathcal{H}}}_0 = \underline{\chi}_0^\dagger \Omega_0$ (owing to the hermiticity of the wave operator[4]) leads to

$$\begin{aligned}
\Omega_1 &= \Omega_{1A} + \Omega_{1B}, && (79)\\
\Omega_{1A} &= \underline{\chi}_0^\dagger \underline{\underline{\mathcal{H}}}_1 \underline{\chi}_0 + \frac{i}{2}\underline{\chi}_0^\dagger \left\{\underline{\underline{\mathcal{H}}}_0, \underline{\chi}_0\right\} + \frac{i}{2}\underline{\chi}_0^\dagger \left\{\underline{\chi}_0, \Omega_0\right\}, && (80)\\
\Omega_{1B} &= -i\underline{\chi}_0^\dagger \left\{\underline{\chi}_0, \Omega_0\right\}. && (81)
\end{aligned}$$

As we will see in the next lectures, those order one correction will play a central role in the reconstruction of the spectrum eigenmodes.

Which terms are gauge dependent? The choice of separating the corrections into a part A and a part B is related to an important point noticed by Littlejohn and Flynn in 1991. Recall that the vectors $\underline{\chi}_0$ solutions of the zeroth order equation are defined up to a phase factor. In physical jargon, choosing this phase amounts to a gauge choice. It appears that the first order expression of the scalar symbol Ω_1 depends on this gauge choice. It is however possible to split the symbol into a part Ω_{1A} that is gauge independent and a part Ω_{1B} that is not gauge independent. This can be checked by applying the transformation $\underline{\chi}_0 \to \underline{\chi}_0 e^{ig(y,p)}$, where $g(y,p)$ an arbitrary real function. The term Ω_{1A} is left unchanged, while the term $\Omega_{1B} \to \Omega_{1B} + \{g, \Omega_0\}$ is shifted.

3.5 Berry corrections to ray tracing equations

Wave packet center of mass and wave packet momentum We define the wavepacket location and wavenumber as an energy-weighted averaged in phase space for the *multicomponent wave* field, which is the physical field to be observed:

$$y_v = \int \mathrm{d}y\ \underline{\Psi}^\dagger \cdot (y\underline{\Psi}), \quad p_v = \int \mathrm{d}y\ \underline{\Psi}^\dagger \cdot (-i\epsilon\partial_y \underline{\Psi}), \tag{82}$$

where the subscript v stands for *vectorial*, and where $\underline{\Psi}$ is normalized according to (70). Recall that this normalisation constraint is equivalent to the energy conservation for shallow water waves.

[4]This is the only step involving the hermicity assumption, which allows to cancel some of the terms. The diagonalization prodecure does not rely on this assumption, and could be performed, albeit with additional terms.

It will be useful to introduce similar quantities defined formally from the scalar wavefield ψ:

$$y_s = \int \mathrm{d}y \ \psi^* \cdot (y\psi), \quad p_s = \int \mathrm{d}y \ \psi^* \cdot (-i\epsilon\partial_y\psi), \tag{83}$$

where the subscript s stands for *scalar*.

WKB ansatz. We now consider the traditional WKB ansatz for the scalar wave field ψ:

$$\psi(y,t) = a_0 e^{\frac{i}{\epsilon}(\phi_0+\epsilon\phi_1)} + \mathcal{O}(\epsilon) \tag{84}$$

where $a_0(y,t)$, $\phi_0(y,t)$ and $\phi_1(y,t)$ are real fields of order ~ 1. This scalar wave field is related to the multicomponent wave field through (69). Using the order zero development of operators acting on a WKB ansatz (as detailed in Appendix 6) leads to

$$\begin{aligned} \underline{\Psi}(y,t) &= a_0 e^{\frac{i}{\epsilon}(\phi_0+\epsilon\phi_1)} \underline{\chi}_0(y,p(y,t)) + \mathcal{O}(\epsilon), & (85)\\ p(y,t) &= \partial_y\phi_0 + \epsilon\partial_y\phi_1. & (86) \end{aligned}$$

Localized wavepacket. We now assume that the wavepacket is localized at y_c over a scale $\Delta y \ll 1$, keeping $\Delta y \gg \epsilon$. Up to higher order terms, we get useful relations

$$\begin{aligned} y_v &= y_s + i\epsilon\underline{\chi}_0^\dagger \cdot \partial_p\underline{\chi}_0 & (87)\\ p_v &= p_s - i\epsilon\underline{\chi}_0^\dagger \cdot \partial_y\underline{\chi}_0 & (88) \end{aligned}$$

The last term on the rhs is gauge dependent: it is not invariant for a change of phase choice in $\underline{\chi}_0$. Since y_v and p_v are quantities built from the initial multicomponent wave problem that does not depend on any phase choice, they are gauge invariant. This means that the coordinates (y_s, p_s) are *not* gauge-invariant.

Ray tracing equations in (y_s, p_s) space. A time differentiation of (83) together with the Hermiticity of the operator $\hat{\Omega}$ leads to:

$$\dot{y}_s = \int \psi^* \widehat{\partial_p\Omega}\psi, \quad \dot{p}_s = -\int \psi^* \widehat{\partial_y\Omega}\psi. \tag{89}$$

Using the WKB ansatz in the limit $\epsilon \to 0$ followed by the localized wavepacket assumption yields

$$\begin{aligned} \dot{y}_s &= +\partial_{p_s}\Omega_s & (90)\\ \dot{p}_s &= -\partial_{y_s}\Omega_s & (91)\\ \Omega_s &= \Omega_0 + \epsilon\Omega_{1A} + \epsilon\Omega_{1B} & (92) \end{aligned}$$

where Ω_s is the symbol of the scalar operator. An unpleasant situation occurs: the ray dynamics in phase space (y_s, p_s) depends on the term Ω_{1B} which depends on the phase choice for $\underline{\chi}_0$.

Ray tracing equations in (y_v, p_v) space. Using the change of variables (87-88) in ray tracing equations (90, 91) leads to a new set of equations:

$$\begin{aligned} \dot{y}_v &= +\partial_{p_v}\Omega_v + \epsilon\mathcal{F}_{yp}\dot{y}_v & (93)\\ \dot{p}_v &= -\partial_{y_v}\Omega_v + \epsilon\mathcal{F}_{yp}\dot{p}_v & (94)\\ \Omega_v &= \Omega_0 + \epsilon\Omega_{1A} & (95) \end{aligned}$$

where $\mathcal{F}_{yp} = -\mathcal{F}_{py}$ is given

$$\mathcal{F}_{yp} = i\{\underline{\chi}_0^\dagger, \underline{\chi}_0\}. \tag{96}$$

This is the definition of a Berry curvature term, as introduced in lecture 1, equation (29). Note that all terms in ray tracing equations (93)-(94) are gauge independent.

3.6 Application to shallow water waves.

We now add back the upperscript $\pm$ to distinguish the two operators of the semi-classical limit $k \to \pm\infty$ introduced at the beginning of this lecture. We restrict ourself to the positive frequency Poincaré inertia-gravity waves (lowerscript index + in lecture 1).

Q) *Check the following expressions*

$$\begin{aligned}
\Omega_0^{\pm} &= \sqrt{y^2+p^2+1} \equiv \omega_0, &(97)\\
\underline{\chi}_0^{\pm} &= \frac{1}{\sqrt{2\omega_0}\sqrt{1+p^2}} \begin{pmatrix} \pm\omega_0 + iyp \\ \omega_0 p \mp iy \\ 1+p^2 \end{pmatrix}, &(98)\\
\Omega_{1A}^{\pm} &= \mp\frac{1}{2\omega_0^2} &(99)\\
\Omega_{1B}^{\pm} &= \mp\frac{y^2}{\omega_0^2\,(1+p^2)} &(100)\\
\mathcal{F}_{yp}^{\pm} &= \mp\frac{1}{\omega_0^3} &(101)
\end{aligned}$$

This last term is related to the first component of the Berry curvature vector introduced in lecture 1, equation (28), and computed explicitly in (30) for the shallow water wave model:

$$\mathcal{F}_{yp}^{\pm} dydp = \left(\lim_{k\to\pm\infty} \mathcal{F}_{fl}\right) f' dydl \tag{102}$$

$$\mathcal{F}_{yp}^{\pm} = \frac{\pm 1}{\sqrt{1+y^2+p^2}^{\,3}} \tag{103}$$

3.7 Bohr-Sommerfeld Quantization

Now that we have projected the multicomponent (vectorial)wave problem into a scalar operator, it is possible to apply the same quantization procedure as in the introductory part of this lecture.

Phase jump in (y_s, p_s)-space. In phase space with coordinates (y_s, p_s), ray trajectories with frequency ω are found by solving

$$\omega = \Omega(y_s, p_s = \partial_{y_s}\phi). \tag{104}$$

Once a trajectory in phase space is known for a given ω, the phase picked up by a wave after a full cycle of is obtained by an integration:

$$\frac{\phi}{\epsilon} = \frac{1}{\epsilon}\oint_{\omega=\Omega(y_s,p_s)} p_s(y)dy + \pi. \tag{105}$$

Phase jump in (y_v, p_v)-space. We explained in previous section that computing trajectories in phase space (y_s, p_s) is awkward, as the computation involves gauge dependent terms. Using (87)-(88) to change variables in the integral (105) leads

$$\frac{\phi}{\epsilon} = \frac{1}{\epsilon}\oint_{\Omega_v(y_v,p_v)=\omega} p_v(y)dy + i\oint_{\Omega_v(y_v,p_v)=\omega} \underline{\chi}_0^{\dagger}\cdot d\underline{\chi}_0 + \pi. \tag{106}$$

See *Littlejohn Flynn PRA 1991* for a detailed derivation. Using Stokes theorem, the second term of the rhs can be expressed as a flux of Berry curvature across the surface delimited by the ray trajectory:

$$\Gamma(\omega) = \iint_{\Omega_v(y_v,p_v)<\omega} \mathrm{d}y_v \mathrm{d}p_v\ \mathcal{F}_{py}(y_v,p_v) \tag{107}$$

with $\mathcal{F}_{py}$ defined in (96).

Finally, we get the following **quantization condition:**

$$\oint_{\Omega_v(y_v,p_v)=\omega} p_v(y_v)dy_v + \epsilon\Gamma(\omega) = 2\pi\epsilon\left(m+\frac{1}{2}\right), \quad m \in \mathbb{Z}. \tag{108}$$

One needs to check a posteriori which values of m lead to admissible solutions.

The key message here is that an integral of Berry curvature over phase space enters in the quantization condition.

3.8 Imbalance of inertia-gravity wave modes in the semi-classical limit

We now use the quantization condition to compare the number of inertia-gravity modes in the limits $k \to \pm\infty$ (operators $\hat{\Omega}^{\pm}$ in the limit $\epsilon \to 0$).

Ray trajectories in phase space (y_v, p_v) are found by solving $\omega = \Omega_v^{\pm}(y_v, p_v)$. This leads to circular trajectories that satisfying the relation

$$\omega = \sqrt{1+\varrho^2} \mp \frac{\epsilon}{2}\frac{1}{1+\varrho^2}, \quad \varrho(\omega) = \sqrt{y_v^2 + p_v^2}. \tag{109}$$

Admissible values $\omega^{\pm}$ are then obtained by applying the quantization relation (108), which leads to

$$n^{\pm} = \frac{1}{2\pi\epsilon}\pi\varrho^2(\omega) + \frac{1}{2\pi}\Gamma^{\pm}(\omega) - \frac{1}{2}, \quad n^{\pm} \in \mathbb{Z}, \tag{110}$$

We now need to find the admissible values of $n^{\pm}$ and to pair them together, based on some physical criterion. For this, it is instructive to look first at the large frequency limit and then at the low radius limit.

Large frequency limit. The principal symbols $\Omega_0^{\pm}$ of the two operators $\hat{\Omega}^{\pm}$ are identical. A direct inspection of their first order correction terms $\Omega_1^{\pm}$ shows that they vanish in the limit $\omega \to +\infty$ (large $n^{\pm}$ limit). This implies that trajectories $\Omega_v^{\pm}(y_v, p_v) = \omega$ are the same in the large frequency limit. Thus the first term in the r.h.s. of (110) is the same for both operators. In addition, the Berry curvature term $\Gamma^{\pm}$ tend to $\pm 2\pi$ in this limit FIGURE. We conclude that

$$\lim_{\omega\to+\infty}\left(n^+ - n^-\right) = 2 \tag{111}$$

Besides, since their symbol converge to a common expression, spectral properties of the corresponding operators $\hat{\Omega}^{\pm}$ are also expected to converge in this limit.

Pairing the modes. The pairing procedure between modes of $\hat{\Omega}^+$ and $\hat{\Omega}^-$ can thus formally be performed by assigning a single index n to their common eigenmodes in the limit $n^{\pm} \to +\infty$. This is done by choosing

$$n^{\pm} = n \pm 1 \tag{112}$$

The term $\pm$ compensate the contributions from the Berry term in the limit $\omega^{\pm} \to +\infty$. Thus, our choice ensures that the value of $\omega^{\pm}$, the solution of the quantization condition (110), are the same for a given n in the limit $n \to +\infty$.

Admissible values for $n^{\pm}$. The first term in the r.h.s. of (110) is an area, it is thus strictly positive. we conclude that $n^{\pm}$ admits a lower bound, which is found by looking at the limit $\varrho \to 0$ FIGURE. First, remember that $\omega^{\pm} > 1 \mp \epsilon/2$, from (109). Second, in the limit $\varrho \to 0$ we get $\Gamma^{\pm}(\omega) = 0$ FIGURE. Consequently, given the choice (112), we get $n^{\pm} \geq 0$ and the conditions

$$n \geq 1 \text{ for eigenfunctions of } \hat{\Omega}^-, \text{ ensuring } n^- \in \mathbb{N}\ , \tag{113}$$

$$n \geq -1 \text{ for eigenfunctions of } \hat{\Omega}^+, \text{ ensuring } n^+ \in \mathbb{N}\ . \tag{114}$$

This means that two modes labeled by $n = -1$ and $n = 0$ are unpaired! This was precisely expected from bulk boundary correspondence. In fact, one can check that

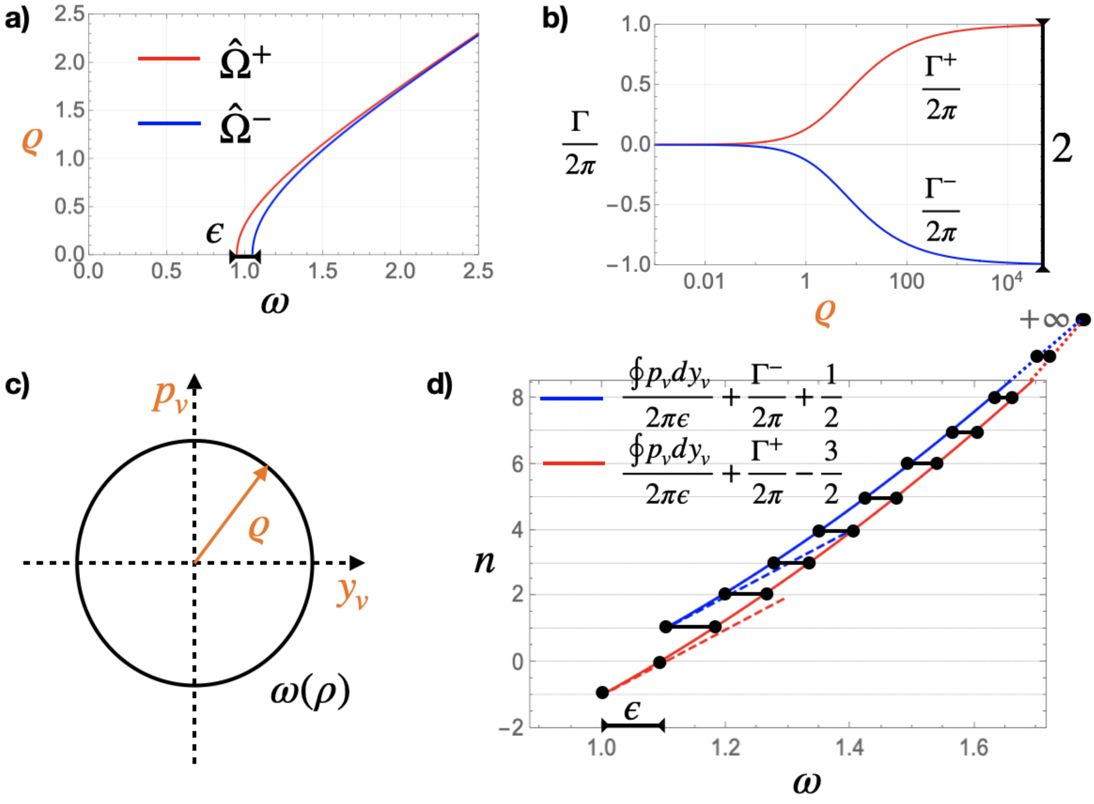

Figure 16: **(a)** Variations of the circular trajectory radius ϱ as a function of frequency ω in phase space (y_v, p_v). **(b)** Variation of the Berry flux across the area delimited by a circular ray trajectory having a radius ϱ. **(c)** A circular trajectory in phase space. **(d)** Quantization condition for shallow water waves in the semi-classical limit, as expressed in (110)-(112). Red and blue curves are associated respectively with operators $\hat{\Omega}^+$ and $\hat{\Omega}^-$. Dashed lines correspond to explicit computations performed in the limit $\epsilon \to 0$ at finite n.

- $n = -1$ is the Kelvin mode
- $n = 0$ is the Yanai (or mixed Rossby-gravity) mode.

To conclude, ray tracing and quantization condition in the imit $\epsilon \to 0$ allow us to recover a semi-classical version of the spectral flow result: just as two modes are gained by the positive frequency Poincaré wave band as k is varied from $-\infty$ to $+\infty$, the operator $\hat{\Omega}^+$ admits two more eigenmodes than the operator $\hat{\Omega}^-$ in the semi-classical limit $\epsilon \to 0$.

3.9 Interpretation of the bulk-interface correspondence

The previous computation shows that the imbalance of 2 modes between operators $\hat{\Omega}^+$ and $\hat{\Omega}^-$ in the semi-classical limit is due to the Berry curvature flux corrections $\Gamma^\pm$ involved in ray tracing equations, with

$$\lim_{\omega \to +\infty} \frac{\Gamma^+(\omega) - \Gamma^-(\omega)}{2\pi} = 2, \tag{115}$$

In fact, (115) can be interpreted as the direct outcome of the Chern-Gauss-Bonnet formula (**??**) that relates an integrated Berry curvature flux to a Chern number.

From phase space to parameter space. Let us consider the parameter space (k, l, f), and a closed cylindrical surface $\mathcal{S}$ oriented in k direction, centered at the origin FIGURE. The length of the cylinder is $2k = 2/\sqrt{\epsilon}$, while its circular ends are delimited by a closed circular ray trajectory

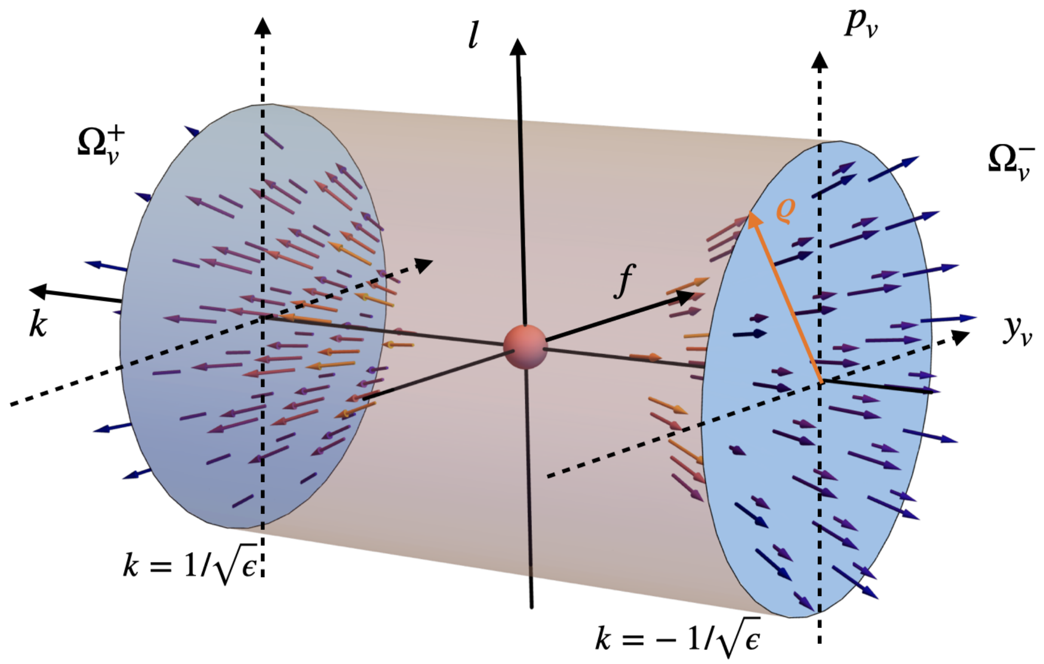

Figure 17: **Parameter space and phase space for ray tracing**. The surface $\mathcal{S}$ in parameter space is a cylinder where both circular ends are delimited by closed phase space trajectories of radius ϱ at positions $k = \pm 1/\sqrt{\epsilon}$.

with a radius $\varrho(\omega)$ in phase space (y_v, p_v), which is related to parameters (k, l, f) through the relation

$$(k, l, f) = |k|(\pm 1, p_v, y_v). \tag{116}$$

From now on we drop the index v.

Chern-Gauss-Bonnet. The surface $\mathcal{S}$ encloses the degeneracy point $(0, 0, 0)$. Recall from lecture 1 that the normalized Berry flux across this surface gives a chern number $\mathcal{C} = 2$ for the positive frequency Poincaré waveband. The integral can then be decomposed into three contributions:

$$\underbrace{\frac{1}{2\pi}\int_{\mathcal{S}_{cyl}} da\mathbf{F}\cdot\mathbf{n}}_{\text{Flux across the open cylinder}} + \underbrace{\frac{1}{2\pi}\int_{\sqrt{y^2+p^2}\leq\varrho} \mathrm{d}y\mathrm{d}p\mathcal{F}_{yp}}_{\text{Flux across the disc at } k=1/\sqrt{\epsilon}} + \underbrace{\frac{1}{2\pi}\int_{\sqrt{y^2+p^2}\leq\varrho} \mathrm{d}y\mathrm{d}p\mathcal{F}_{yp}}_{\text{Flux across the disc at } k=-1/\sqrt{\epsilon}} \tag{117}$$

where we have used $\mathcal{F}_{fl}\mathrm{d}f\mathrm{d}l = \mathcal{F}_{yp}\mathrm{d}y\mathrm{d}p$, consistently with the definition of Berry curvature in (29).

From Berry fluxes to the mode imblance To estimate the three contributions in (117), we consider a double limit whose order matters: first, the limit of infinite radius $\varrho \to +\infty$ for a given value of k ; second, the semi-classical limit $k \to \pm\infty$. The first limit allows to get properties of the full spectrum for a given value of k, by scanning all possible trajectories in phase space (y, p). The second limit allows us to get asymptotic properties of this full spectrum in the semi-classical limit.

The first limit $\varrho \to +\infty$ implies that the contribution of Berry flux across the open cylinder surface $\mathcal{S}_{cyl}$ vanishes. Once this limit has been taken, the only non-zero contribution to the Berry flux across $\mathcal{S}$ comes from the two circular surfaces at the ends of the cylinder. The Berry flux across those surfaces only involve the component $\mathcal{F}_{yp}dydp$ which tends to $\mathcal{F}^{\pm}_{yp}dydp$ when taking the limit $k \to \pm\infty$. Finally, we get

$$\lim_{\epsilon\to 0}\lim_{\omega\to+\infty}\frac{1}{2\pi}\int_{\mathcal{S}} \mathrm{d}a\mathbf{F}\cdot\mathbf{n} = \lim_{\omega\to+\infty}\frac{\Gamma^+(\omega) - \Gamma^-(\omega)}{2\pi} = \mathcal{C}. \tag{118}$$

This shows the topological origin of the r.h.s. integer term in (115).

The message is that ray tracing followed by quantization in an appropriate semi-classical limit offers a physically appealing intuitive explanation on the relation between the topological index and the spectral properties of the operator.

3.10 Reading material

- The WKB method is well introduced and detailed in the bnook *Bender and Orzag, Advanced mathematical methods for scientists and engineers.* A good introduction to ray tracing in geophysical context is *Buhler, Waves and mean fllows CUP*
- The classic paper on ray tracing and Berry curvature is *Littlejohn and Flynn 1991 Physical review A*
- A geophysical manifestation of this effect is presented in *Perez et al 2021 Proc. Roy. Soc.*.
- This chapter is a shortened version of a preprint *Venaille, Onuki, Perez, Leclerc 2022*, Arixv July 2022.

Conlusion

(Slides)

Main message of the lecture: Simple properties of complicated wave problem can be predicted using tools from topology. Local dispersion relation is not enough: important information is also encoded in the polarization relation.

Important concepts introduced in these lectures:

- Berry curvature
- Chern number
- Spectral flow
- Bulk-interface correspondence (index theorem)
- Wigner-Weyl transform and symbolic calculus
- Ray tracing

We focused on a specific problem (inviscid shallow water waves) to present a general method. The same tools can be applied to a variety of physical systems. Important additional topic not covered in these lectures:

- Non hermitian effects
- Nonlinear effects
- Applications to plasma
- Applications to asteroseismology
- Applications to active matter

4 Appendix to lecture 1: mapping shallow water dynamics to ocean and atmospheric flows

In the lectures, we consider a shallow water model with a free interface between the fluid layer and air. Let us explain briefly how this model can be conveniently used to describe the propagation of temperature anomalies in the upper ocean, or planetary waves in the atmospheres, which turn out to be surprising well described by linear shallow water theory, even if atmosphere is a stratified gas rather. than a fluid layer.

Temperature anomalies at ocean surface and laboratory realization of Coastal Kelvin waves

We argued that temperature anomalies propagating along the Pacific is a topological equatorial Kelvin wave? How does it relate to to the shallow water model presented here?

To understand the shallow water interpretation of the planetary heat wave observed in the upper ocean figure 1, one needs to consider a two-layer shallow water model, each of the layer having a different density, or, equivalently a different temperature, as illustrated figure 18. The upper layer is assumed to be active, while the lower layer is assumed to be at rest. In the ocean, the upper layer with high temperature (low density) is called the thermocline, while the lower, denser layer represents the cold abyss.

Variations of the upper layer depth is dominated by the fluctuations of the internal interface: such interface is indeed easy to perturb as is involves weak density variations between both layers ($\Delta\rho/\rho \ll 1$) in the ocean. At lowest order, the dynamics of this upper layer is then described by equation (), provided that g is replaced by the reduced gravity $g' = \Delta\rho/\rho$. Consequently, the phase speed of internal interface waves $c = \sqrt{g'H}$ is much smaller than the surface waves. Another important consequence is that the trapping length scale of the equatorial waves of the internal interface is much smaller than the trapping length scale of surface wave.

In this framework, positive temperature anomalies observed in the upper ocean can then be interpreted as large upper ocean layer thickness. The table top laboratory experiment of Sakai presented during the lecture is also based on a two layer system, with waves being forced in the upper layer. The advantage with respect to single layer systems is to obtain smaller phase speeds, and smaller trapping length scales by playing with reduced gravity:

https://www.gfd-dennou.org/library/gfd_exp/exp_e/exp/kw/index.htm
[5].

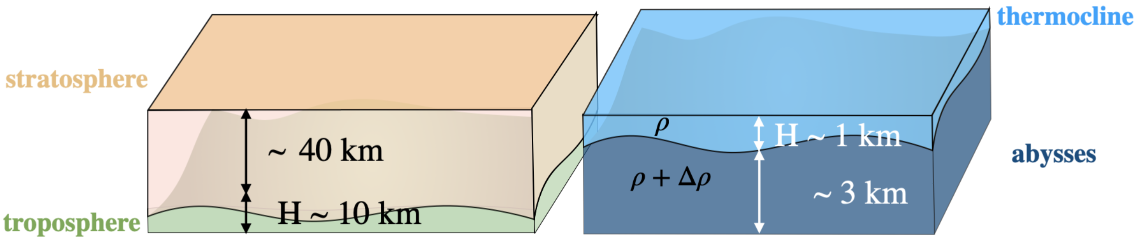

Figure 18: Two layer interpretation of ocean and atmosphere. A shallow water model can be used to describe the thermocline, considered as a layer of homogeneous density on the top of another, denser layer at rest. While a similar structure occurs in the atmosphere with the troposphere playing the role of a thermocline, the shallow water interpretation of planetary atmospheric waves requires to project the dynamics into vertical modes. Figure adapted from *Delplace Venaille La Gazette des mathématiques 2019*

[5] En réalité, des ondes se propagent aussi dans les abysses et la stratosphère et l'analyse fine des observations requiert la prise en compte de la stratification continue en densité de ces écoulements.

Wheeler Kiladis spectra in the atmosphere

This part is adapted from a chapter on atmospheric equatorial waves in ISTE encyclopedia, withh J. Dias and Y-M. Cheng, to be published in 2023.

Amazingly, linear theory of Matsuno presented in lecture 1can be used to describe many features of atmospheric frequency-wavenumber power spectra. A spectacular demonstration was given by Wheeler and Kiladis at the end of the nineties. This is illustrated in figure 19.

Continuously stratified fluids. It is a priori not obvious to relate the shallow water model of lecture 1 to an actual atmosphere. For instance, what would be the fluid depth in this framework? As we shall see, shallow water waves emerge naturally from more complicated flow models. To proceed, we start by addressing the role of density stratification on equatorial waves, by considering a linearized hydrostatic (Boussinesq) flow model linearized around a state of rest:

$$\begin{aligned} \partial_t u' &= -\partial_x \phi + f v', \\ \partial_t v' &= -\partial_y \phi' - f u', \\ 0 &= -\partial_z \phi' + b', \\ 0 &= \partial_x u' + \partial_y v' + \partial_z w', \\ \partial_t b' &= -w' N^2. \end{aligned} \tag{119}$$

We have introduced the buoyancy perturbation b', the geopotential ϕ' that can be interpreted as a perturbation to hydrostatic pressure, and and the buoyancy frequency $N^2 \equiv \partial_z \bar{b}$ with $\bar{b}(z)$ the buoyancy profile of the base state. The third equation is hydrostatic balance, the fourth equation is the incompressibility condition, and the last equation is buoyancy advection.

For the sake of simplicity, we assume now that the buoyancy frequency N does not depends of z, and that the domain is infinite in the z-direction. We obtain a direct mapping with the shallow water dynamics by considering

$$\left(\frac{u'}{c_m}, \frac{v'}{c_m}, \frac{\phi'}{c_m^2}\right) = (u'_m, v'_m, \phi'_m) e^{imz}, \quad c_m \equiv \frac{N}{|m|} \tag{120}$$

One can check that the dynamics of the triplet (u'_m, v'_m, ϕ'_m) is ruled by en effective shallow water model (9), assuming $\eta' = \phi'_m$ and $c = c_m$.

Shallow water interpretation. When mapping the hydrostatic Boussinesq model to a shallow water model, the geopotential field is interpreted as an effective height field. According to hydrostatic balance in Eq. (119), the perturbed geopotential field is proportional to the perturbed buoyancy field: $im\phi'_m = b'_m$. Since buoyancy variations are mainly driven by temperature variations, one can interpret each projection of a temperature anomaly field onto vertical modes as the height field of an effective shallow water model.

The concept of equivalent depth. The horizontal phase speed c_m of nonrotating hydrostatic Boussinesq waves with vertical wavenumber m can be interpreted in terms of an equivalent depth. This would be the depth of a shallow water model supporting similar horizontally propagating waves:

$$h_{eq} \equiv \frac{1}{g} \frac{N^2}{m^2}, \quad c_m = \sqrt{g h_{eq}} \tag{121}$$

In practice, wave properties extracted from observed horizontal fields are often interpreted by considering the equivalent depth h_{eq} as a fitting parameter, which amounts here to assume that the dynamics projects well on a single vertical mode.

To obtain the order of magnitude of h_{eq} for the Earth atmosphere, we assume that deep convection sets a vertical wavenumber $m = \pi/H$ with $H = 15$ km the typical height of the troposphere. The buoyancy frequency is of the order of $N = 10^{-2}$ s^{-1}, and $g = 10$ m.s^{-1}, which, using (121), leads to the dry atmosphere equivalent depth $h_{eq} = 250$ m, with typical phase speed $c_m = 50$ m.s^{-1}.

Horizontal structure of an atmospheric Kelvin wave. Once spectral peaks are identified, a spectral filter can be applied to the data to retain only the spectral coefficients associated with

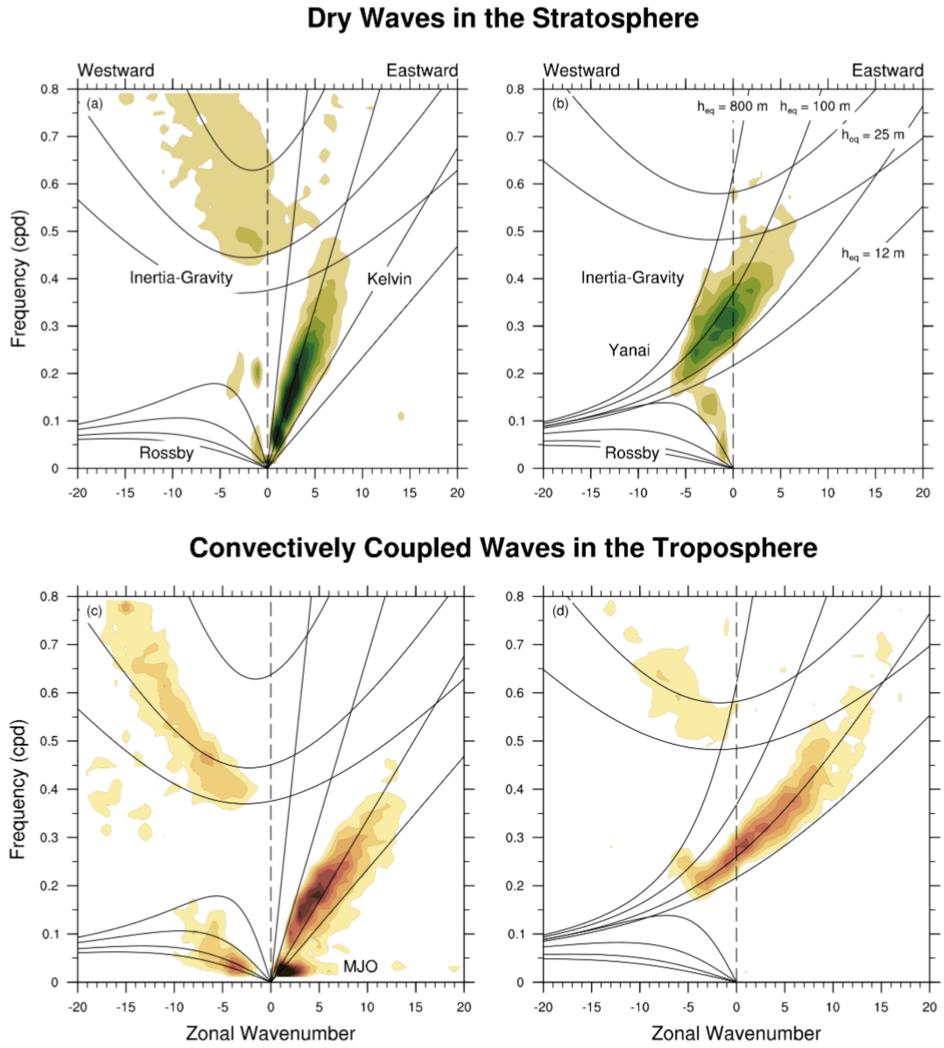

Figure 19: Wave number-frequency power spectrum of equatorial data averaged from 15S to 15N displayed as the ratio between the raw and smoothed red noise background spectrum *(details in Wheeler and Kiladis JAS 1999)*. The top panel demonstrates waves in the stratosphere as power spectra of zonal wind from ERA5 reanalysis (which use both observations and a numerical model). The bottom panel shows waves in the troposphere as spectra of brightness temperature from satellite observation, which is related to cloud cover (cloud generally means upward vertical velocity, which can be related to horizontal convergence. In both panels, the data are decomposed into meridionally symmetric (left) and antisymmetric (right) components. Dispersion curves are overlaid for equivalent shallow water depths of 12, 25, 100, and 800 m. See text of the appendix for the interpretation of this equivalent depth and see figure 18 for definition of the troposphere and stratosphere. The spectral peak off the dispersion relation in the troposphere corresponds to MAdden Julian Osillation, a phenomenon for which there is still no commonly accepted explanation *Courtesy of J. Dias and Y-M. Cheng*

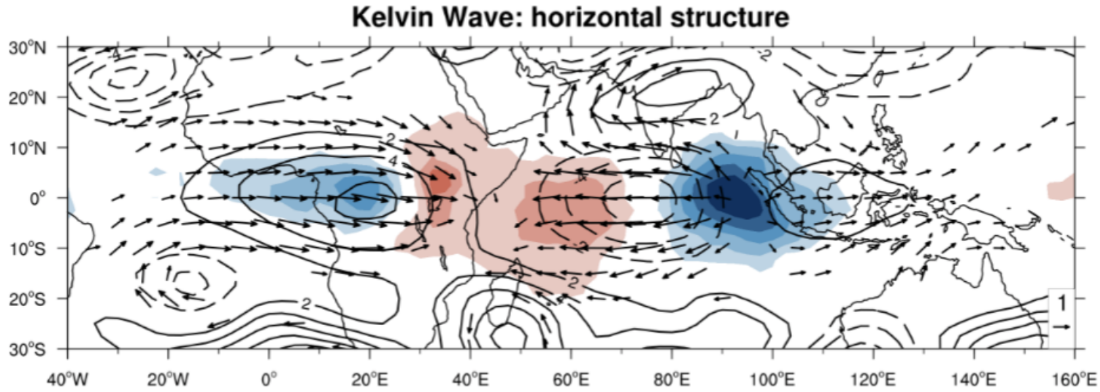

Figure 20: Reconstruction of the flow pattern associated with frequency and wavenumber close to a spectral peak associated with Kelvin waves in Wheeler-Kiladis spectrum. Compare to figure 6: the observed pattern is strikingly similar to the one originally computed by Matsuno in the shallow water case.

those peaks. A remarkable outcome of this methodology is that these inferred patterns share strong similarities with the modes of equatorial waves computed originally by Matsuno. For instance, the horizontal structure of the idealized Kelvin waves plotted in figure 6 is close to the observed pattern figure **??**, where the equatorial geopotential height and zonal winds are roughly in phase and zonal winds are the dominant wind component.

5 Appendix to lecture 2: topology of eigenmode bundles enclosing two-band degeneracy points.

This subsection can be skipped if you accept that the Chern number of generic two-fold degeneracy point is ± 1.

Let us zoom on any of the two-band degeneracy point introduced in previous subsection, say for instance the one at $\beta_t = ck = f$, and let us introduce a vector of parameters denoted $\boldsymbol{\lambda} \in \mathbb{R}^3$ that vanishes at the degeneracy point:

$$\boldsymbol{\lambda} = (k, l, \beta_t) - (f/c, 0, f). \tag{122}$$

Sufficiently close to the degeneracy point, the two-band crossing problem is described by a reduced 2×2 matrix, which, owing to the hermitian nature of the problem, can always be written as

$$H_r(\boldsymbol{\lambda}) = \begin{pmatrix} h_3(\boldsymbol{\lambda}) & h_1(\boldsymbol{\lambda}) - ih_2(\boldsymbol{\lambda}) \\ h_1(\boldsymbol{\lambda}) + ih_2(\boldsymbol{\lambda}) & -h_3(\boldsymbol{\lambda}) \end{pmatrix} \tag{123}$$

where $\boldsymbol{h}(\boldsymbol{\lambda}) = (h_1, h_2, h_3) \in \mathbb{R}^3$ depends linearly on the components of $\boldsymbol{\lambda}$, with

$$\boldsymbol{h}(\boldsymbol{\lambda} = 0) = 0 \tag{124}$$

Q) *Let us for a moment forget the dependence on* $\boldsymbol{\lambda}$*, and consider* $\mathbf{h}$ *as a parameter. Use the same method as in lecture 1 to show that the Chern number of the two eigenmode bundles parameterized over a spherical closed surface* $\Sigma_{\mathbf{h}}$ *enclosing the degeneracy point* $\mathbf{h} = 0$ *are*

$$\mathcal{C}_h^{\pm} = \frac{1}{2\pi} \int_{\Sigma_{\mathbf{h}}} \mathbf{F}^{(\pm)}(\mathbf{h}) \cdot \mathrm{d}\boldsymbol{\Sigma}_{\mathbf{h}} = \mp 1, \tag{125}$$

where $\mathbf{F}^{(\pm)}(\mathbf{h})$ *is the Berry curvature associated with the two eigenmodes denoted* $\underline{\Psi}^{\pm}$.

Now, we want to compute the Chern number for the eigenmode bundles defined on a surface denoted $\Sigma_{\boldsymbol{\lambda}}$ in $\boldsymbol{\lambda}$-parameter space rather than in $\mathbf{h}$-space. We assume that the surface $\Sigma_{\boldsymbol{\lambda}}$ encloses the band crossing point $\boldsymbol{\lambda}=0$. We introduce the degree $\deg h$ that counts how many times the application $h:\ \boldsymbol{\lambda}\in\Sigma_{\boldsymbol{\lambda}}\rightarrow \boldsymbol{h}/|\boldsymbol{h}|\in\Sigma_{\boldsymbol{h}}$ wraps the unit sphere in $\mathbf{h}$-parameter space when $\boldsymbol{\lambda}$ is varied over $\Sigma_{\boldsymbol{\lambda}}$. Here, there is a non-singular linear transformation from $\boldsymbol{\lambda}$ to $\mathbf{h}$, so that $\mathbf{h}/|\mathbf{h}|$ wraps one time the sphere S^2 when $\boldsymbol{\lambda}$ wraps the surface $\Sigma_{\boldsymbol{\lambda}}$:

$$|\deg(h)|=1 \tag{126}$$

The sign of $\deg(h)$ accounts for a possible change orientation induced by the linear transformation. A direct computation of the Chern number through the integral of Berry curvature in $\boldsymbol{\lambda}$-parameter space yields finally to

$$\mathcal{C}_{\pm}=\frac{1}{2\pi}\int_{\Sigma_{\boldsymbol{\lambda}}}\mathbf{F}^{(\pm)}(\boldsymbol{\lambda})\mathrm{d}\boldsymbol{\Sigma}_{\boldsymbol{\lambda}}=\frac{1}{2\pi}\int_{h(\Sigma_{\boldsymbol{\lambda}})}\mathbf{F}^{(\pm)}(\boldsymbol{h})\mathrm{d}\boldsymbol{\Sigma}_{\boldsymbol{h}}=(\deg h)\,\mathcal{C}_h^{\pm} \tag{127}$$

Consequently, the Chern numbers of the eigenmode bundles enclosing the degeneracy point is ± 1.

6 Appendix to lecture 3: symbolic calculus in a nutshell

Symbolic calculus allows to make a correspondence between phase-space dynamics and spectral properties of an operator, through the use of the Weyl-Wigner transform. This appendix gives the definition and some important properties of the Weyl-Wigner transform. It follows closely the presentation given in a paper by *Onuki (JFM 2020)*.

Wigner-Weyl transform

Definitions. The Weyl transform is a quantization procedure to define an operator $\hat{f}(y,\partial_y)$ from the knowledge of a (phase space) function $f(y,p)$, which is called the symbol of $\hat{f}$. When applied to a test function $\psi(y)$, the Weyl transform is defined as

$$\hat{f}\psi(y)=\frac{1}{2\pi\epsilon}\int \mathrm{d}y'\mathrm{d}p\ e^{i\frac{p}{\epsilon}(y-y')}f\left(\frac{y+y'}{2},p\right)\psi(y') \tag{128}$$

Note that the $\hat{f}$ can formally be written with an integral representation as

$$\hat{f}\psi(y)=\int \mathrm{d}y'\ F(y,y')\psi(y') \tag{129}$$

Using those definitions, on can check that the symbol is recovered through a Wigner transform applied to $F(y,y')$:

$$f(y,p)=\int \mathrm{d}y'\ F\left(y+\frac{y'}{2},y-\frac{y'}{2}\right)e^{-\frac{i}{\epsilon}py'} \tag{130}$$

Symbolic calculus make use of those transforms to switch back and forth from operators to symbols.

Interpretation. To see the origin of Weyl quantization procedure, it is useful to introduce the Fourier transform of the symbol

$$\tilde{f}(\eta,\xi)\ =\ \int \mathrm{d}y\mathrm{d}p\ f(y,p)e^{-\frac{i}{\epsilon}(y\eta+p\xi)} \tag{131}$$

$$f(y,p)\ =\ \frac{1}{2\epsilon\pi}\int \mathrm{d}\eta\mathrm{d}\xi\ \tilde{f}(\eta,\xi)\ e^{\frac{i}{\epsilon}(y\eta+p\xi)} \tag{132}$$

The operator $\hat{f}$ is recovered by replacing p with $-i\epsilon\partial_y$ in this last expression:

$$\hat{f}(y,\partial_y)=\frac{1}{2\epsilon\pi}\int \mathrm{d}\eta\mathrm{d}\xi\ \tilde{f}(\eta,\xi)\ e^{\frac{i}{\epsilon}\eta y+\xi\partial_y} \tag{133}$$

To check that (133) is equivalent to (128), recall two useful formula involving the exponential function of operator derivative ∂_y:

$$e^{\xi\partial_y}\psi(y) = \psi(y+\xi), \tag{134}$$
$$e^{i\frac{\eta}{\epsilon}y+\xi\partial_y} = e^{i\frac{\eta\xi}{2\epsilon}}e^{i\frac{\eta}{\epsilon}y}e^{\xi\partial_y}. \tag{135}$$

Expression (133) highlights the original motivation for Weyl quantization, and its difference with other quantization procedures. Indeed, starting from (132), another quantization procedure could have been to replace $e^{\frac{i}{\epsilon}(y\eta+p\xi)}$ by $e^{\frac{i}{\epsilon}y\eta}e^{\xi\partial_y}$, which, according to (135), would lead to a different operator than (133) .

Interest of Weyl quantization. The main interest of the Weyl quantization procedure is that Hermitian scalar operators are mapped to real functions for their symbols. Similarly Hermitian multicomponent wave operators are mapped to Hermitian matrices for their symbol.

Products and commutation rules

One can check that $\hat{p} = -i\epsilon\partial_y$, and $\widehat{g(y)} = g(y)$, meaning that the symbol of the operators $-i\epsilon\partial_y$ and $g(y)$ are p and $g(y)$, respectively. One can also deduce from the definition of Weyl transform and an integration by part that

$$y\hat{f} - \hat{f}y = i\epsilon\widehat{\partial_p f} \tag{136}$$
$$\partial_y\hat{f} - \hat{f}\partial_y = \widehat{\partial_y f} \tag{137}$$

In general, taking the Weyl transform of a symbol product fg does yield to the standard product of corresponding operators $\hat{f}\hat{g}$. It is however possible to define a new product operator at the level of symbol, called star product, or Moyal product, such that

$$\hat{f}\hat{g} = \widehat{f\star g}. \tag{138}$$

The operator product is conveniently written in terms of the Fourier transform of their symbol using (133), followed by (135):

$$\hat{f}\hat{g} = \int \mathrm{d}\eta\mathrm{d}\xi\mathrm{d}\eta'\mathrm{d}\xi'\tilde{f}(\eta,\xi)\tilde{g}(\eta',\xi')e^{\frac{i}{\epsilon}\eta y+\xi\partial_y}e^{\frac{i}{\epsilon}\eta' y+\xi'\partial_y}, \tag{139}$$
$$= \int \mathrm{d}\eta\mathrm{d}\xi\mathrm{d}\eta'\mathrm{d}\xi'\tilde{f}(\eta,\xi)\tilde{g}(\eta',\xi')e^{\frac{i}{2\epsilon}(\eta'\xi-\eta\xi')}e^{\frac{i}{\epsilon}(\eta+\eta')y+(\xi+\xi')\partial_y}, \tag{140}$$
$$= \int \mathrm{d}\eta''\mathrm{d}\xi''\widetilde{f\star g}(\eta'',\xi'')e^{\frac{i}{\epsilon}\eta'' y+\xi''\partial_y}, \tag{141}$$

where the last equality is just the definition of the Weyl transform combined to (138). Identifying the last two lines leads to

$$\widetilde{f*g}(\eta'',\xi'') = \int \mathrm{d}\eta\mathrm{d}\xi\mathrm{d}\eta'\mathrm{d}\xi'\tilde{f}(\eta,\xi)\tilde{g}(\eta',\xi')e^{\frac{i}{2\epsilon}(\eta'\xi-\eta\xi')}\delta(\xi''-\xi'-\xi)\delta(\eta''-\eta'-\eta). \tag{142}$$

It is useful to expand the exponential term as

$$e^{\frac{i}{2\epsilon}(\eta'\xi-\eta\xi')} = \sum_{(n,m)\in\mathbb{N}^2}\frac{(-1)^n}{n!m!}\left(\frac{i}{2}\epsilon\right)^n\left(\frac{i\eta}{\epsilon}\right)^m\left(\frac{i\xi}{\epsilon}\right)^n\left(\frac{i\eta'}{\epsilon}\right)^n\left(\frac{i\xi'}{\epsilon}\right)^m. \tag{143}$$

Basic properties of inverse Fourier transforms finally leads to

$$f\star g = \sum_{(n,m)\in\mathbb{N}^2}\frac{(-1)^n}{n!m!}\left(\frac{i}{2}\epsilon\right)^{n+m}\left(\partial_y^m\partial_p^n f\right)\left(\partial_y^n\partial_p^m g\right). \tag{144}$$

This generalizes the result (**??**) to arbitrary order in ϵ. Note also that (144) is valid for any ϵ if f or g are polynomials in (y,p).

Symbolic calculus with a WKB ansatz

We recall classical results on the asymptotic development of an operator $\hat{L}$ with symbol L acting on a scalar field

$$\psi = a(y)e^{i\frac{\phi(y)}{\epsilon}} \tag{145}$$

This is just a translation in our notations for the particular one-dimensional case. Using the definition (128) together with a change of variable $y'' = y' - y$ leads to

$$\hat{f}\psi(y) = \frac{1}{2\pi\epsilon}\int \mathrm{d}y''\mathrm{d}p\ f\left(y + \frac{y''}{2}, p\right) a(y+y'')e^{\frac{i}{\epsilon}(\phi(y+y'')-y''p)} \tag{146}$$

A Taylor expansion of f, a and ϕ in terms of y'' (that will be justified a posteriori) yields

$$\hat{f}\psi(y) = \frac{\psi(y)}{2\pi\epsilon}\int \mathrm{d}y''\mathrm{d}p\ \left(f + y''\left(\frac{\partial_y f}{2} + \frac{f\partial_y a}{a}\right) + \mathcal{O}(y''^2)\right) e^{\frac{i}{\epsilon}\left((\partial_y\phi - p)y'' + \frac{\partial_{yy}\phi}{2}y''^2 + \mathcal{O}\left(y''^3\right)\right)} \tag{147}$$

where all functions inside the integral are evaluated at y. The term in the exponential is expanded up to order 2 because of the $1/\epsilon$ prefactor. Powers of y in the integrand can be replaced by derivatives with respect to p in front of the exponential term. Keeping only terms up to order ϵ yields to:

$$\hat{f}\psi(y) = \frac{\psi(y)}{2\pi\epsilon}\int \mathrm{d}y''\mathrm{d}p\ \left(f + i\epsilon\left(\frac{\partial_y f}{2} + \frac{f\partial_y a}{a}\right)\partial_p - i\epsilon f\frac{\partial_{yy}\phi}{2}\partial_{pp} + \mathcal{O}(\epsilon^2)\right) e^{\frac{i}{\epsilon}(\partial_y\phi - p)y''} \tag{148}$$

We now expand the symbol, the amplitude and phase functions as

$$f = f_0(y,p) + \epsilon f_1(y,p) + \mathcal{O}(\epsilon^2), \quad a = a_0(y) + \mathcal{O}(\epsilon), \quad \phi = \phi_0(y) + \epsilon\phi_1(y) + \mathcal{O}(\epsilon^2). \tag{149}$$

After integrations by parts for the variable p in Eq (148), and after using the identity

$$\frac{1}{2\pi\epsilon}\int \mathrm{d}y''\ g(y,p)e^{\frac{i}{\epsilon}(\partial_y\phi - p)y''} = g(y,\partial_y\phi)\delta\left(\partial_y\phi - p\right), \tag{150}$$

with $\delta(x)$ the Dirac distribution, we find

$$\hat{f}\psi = f_0\psi + \epsilon\left(f_1 - \frac{i}{2}\left(\partial_{pp}f_0\partial_{yy}\phi_0 + \partial_{yp}f_0 + \partial_p f_0\partial_y\ln(a_0^2)\right)\right)\psi + \mathcal{O}(\epsilon^2) \tag{151}$$

where the symbols f_0 and f_1 are evaluated at $(y, p(y))$ with

$$p = \partial_y\phi_0 + \epsilon\partial_y\phi_1. \tag{152}$$